Resource

Cell Reports

A Chaperome Subnetwork Safeguards Proteostasis in Aging and Neurodegenerative Disease

Graphical Abstract

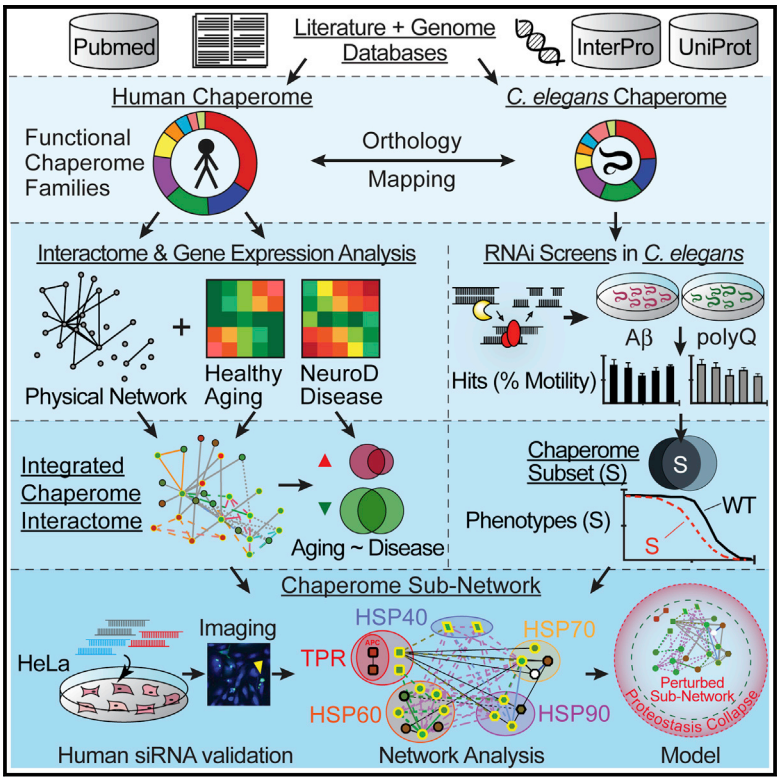

Highlights

Chaperome expression is dramatically affected in human brain aging

Chaperome dynamics correlate with aging and neurodegenerative disease

Functional analysis identifies a chaperome subset that safeguards proteostasis

Authors

Marc Brehme, Cindy Voisine, ..., Hui Ge, Richard I. Morimoto

Correspondence

marc_vidal@dfci.harvard.edu (M.V.), hui.ge@novartis.com (H.G.), r-morimoto@northwestern.edu (R.I.M.)

In Brief

Brehme et al. have examined the chaperome from *C. elegans* to humans using functional assays and expression as well as protein-interactome analysis. The authors identify a conserved *C. elegans* chaperome subnetwork of 16 chaperone genes, corresponding to 28 human orthologs that are affected in brain aging and diseases associated with protein aggregation.

Brehme et al., 2014, Cell Reports 9, 1135–1150
November 6, 2014 ©2014 The Authors
http://dx.doi.org/10.1016/j.celrep.2014.09.042

Cell Reports
Resource

A Chaperome Subnetwork Safeguards Proteostasis in Aging and Neurodegenerative Disease

Marc Brehme,[1,2,3,4,5,6] Cindy Voisine,[4,5,7] Thomas Rolland,[2,3] Shinichiro Wachi,[1] James H. Soper,[1] Yitan Zhu,[1] Kai Orton,[4] Adriana Villella,[1] Dan Garza,[1] Marc Vidal,[2,3,*] Hui Ge,[1,*] and Richard I. Morimoto[4,*]
[1]Proteostasis Therapeutics, Inc., Cambridge, MA 02139, USA
[2]Center for Cancer Systems Biology (CCSB) and Department of Cancer Biology, Dana-Farber Cancer Institute, Boston, MA 02215, USA
[3]Department of Genetics, Harvard Medical School, Boston, MA 02115, USA
[4]Department of Molecular Biosciences, Rice Institute for Biomedical Research, Northwestern University, Evanston, IL 60208, USA
[5]Co-first author
[6]Present address: CeMM Research Center for Molecular Medicine of the Austrian Academy of Sciences, 1090 Vienna, Austria
[7]Present address: Department of Biology, Northeastern Illinois University, Chicago, IL 60625, USA
*Correspondence: marc_vidal@dfci.harvard.edu (M.V.), hui.ge@novartis.com (H.G.), r-morimoto@northwestern.edu (R.I.M.)
http://dx.doi.org/10.1016/j.celrep.2014.09.042

SUMMARY

Chaperones are central to the proteostasis network (PN) and safeguard the proteome from misfolding, aggregation, and proteotoxicity. We categorized the human chaperome of 332 genes into network communities using function, localization, interactome, and expression data sets. During human brain aging, expression of 32% of the chaperome, corresponding to ATP-dependent chaperone machines, is repressed, whereas 19.5%, corresponding to ATP-independent chaperones and co-chaperones, are induced. These repression and induction clusters are enhanced in the brains of those with Alzheimer's, Huntington's, or Parkinson's disease. Functional properties of the chaperome were assessed by perturbation in *C. elegans* and human cell models expressing Aβ, polyglutamine, and Huntingtin. Of 219 *C. elegans* orthologs, knockdown of 16 enhanced both Aβ and polyQ-associated toxicity. These correspond to 28 human orthologs, of which 52% and 41% are repressed, respectively, in brain aging and disease and 37.5% affected Huntingtin aggregation in human cells. These results identify a critical chaperome subnetwork that functions in aging and disease.

INTRODUCTION

The proteomes of eukaryotic cells and tissues are represented by a collection of structurally and functionally diverse proteins that form protein-protein interaction networks to communicate within and between cells and tissues to achieve cellular healthspan and organismal lifespan (Gavin et al., 2006). Protein quality control mechanisms such as the proteostasis network (PN) protect proteome functionality and prevent accumulation of mutant, misfolded, and damaged proteins (Balch et al., 2008). Protein aggregation has profound consequences on cellular and organismal health and can cause both gain of function and loss of function (Park et al., 2013; Yu et al., 2014).

Protein conformational diseases are widespread and include cancer and metabolic and neurodegenerative disorders (Haass and Selkoe, 2007; Powers et al., 2009; Xu et al., 2011). Whereas pathogenic pathways for neurodegenerative diseases such as Alzheimer's (AD), Huntington's (HD), and Parkinson's (PD) intersect (Ehrnhoefer et al., 2011), the clinical profiles and environmental and genetic risk factors vary substantially (Langbehn et al., 2004; Belin and Westerlund, 2008; Hampel et al., 2010). For neurodegenerative diseases, the most significant and universal risk factor is aging; moreover, evidence suggests a mechanistic link between aging, aggregation-mediated proteotoxicity, and loss of proteostasis, which has been put forth as one of the nine hallmarks of aging (Cohen et al., 2006; López-Otín et al., 2013). The accumulation of proteotoxic species during aging is inversely correlated with age-associated proteostasis decline (Ben-Zvi et al., 2009). Chronic expression of misfolded proteins in age-onset neurodegenerative disease leads to accumulation of misfolded species and aggregates that overwhelm proteostasis as a basis of cellular dysfunction (Gidalevitz et al., 2006; Douglas and Dillin, 2010).

A central component of the PN is molecular chaperones and co-chaperones that determine the cellular folding environment, prevent misfolding, and redirect nonnative intermediates to the native state (Hartl et al., 2011) or for clearance by the ubiquitin-proteasome system and autophagy (Schmidt and Finley, 2014). The "chaperome" corresponds to the ensemble of chaperones and co-chaperones that interact in a complex network of molecular folding machines to regulate proteome function (Albanèse et al., 2006). An understanding of the chaperome will be instrumental to the biology of aging and how loss of proteostatic control increases the risk for protein conformational diseases. Whereas much is known about the function of individual chaperones (Hartl et al., 2011), there is only a limited analysis of chaperome dynamics and connectivity in metazoans. We therefore compiled the human and *C. elegans* chaperome by a systematic literature search as a basis for integration of human protein-protein interactions (PPIs) and aging brain expression data to achieve a chaperome interactome network. This was

complemented by functional chaperome-wide RNAi screens in *C. elegans* models of Aβ and polyQ proteotoxicity and a human cellular model of Huntingtin aggregation.

Our study has identified chaperone clusters that exhibit striking repression and induction expression patterns in human brain aging. Repression predominates and involves all major families of cytosolic chaperones with a preponderance of ATP-dependent chaperones. We observed concordance of these dynamics with expression in brain tissues of AD, HD, and PD patients. The correlation of these dynamics underlines the central role of the chaperome in aging and disease. The complement of informatics with experimentation identified a chaperome subnetwork that safeguards cellular and organismal proteostasis in *C. elegans* models and human tissue culture cells expressing neurodegenerative disease-related misfolded proteins. This emergence of a conserved chaperome subnetwork provides a resource for future studies to establish how changes in the PN affect aging and disease.

RESULTS

Composition of the Human Chaperome

We examined the expression of genes encoding molecular chaperones in human brains during normal aging and in neurodegenerative disease. For this, we compiled a list of all human chaperones and co-chaperones by combining the extensive literature on the biochemical properties of molecular chaperones together with curation and structural genomics profiling to match genes by InterPro protein domain identifiers (IPR-IDs) (Hunter et al., 2012; Figure 1A; Table S1). This analysis identified 332 genes (Figure 1A; Tables S1 and S2A; Supplemental Experimental Procedures) that were unambiguously placed into nine chaperone gene families, corresponding to heat shock protein 90 (HSP90), HSP70, HSP60, HSP40, prefoldin, small HSPs (sHSPs), tetratricopeptide repeat (TPR)-domain-containing (Hartl and Hayer-Hartl, 2002), and organellar-specific chaperones of the ER (Kleizen and Braakman, 2004) and mitochondria (MITO) (Tatsuta et al., 2005). For genes with matching IPR-criteria domains, the groupings were prioritized by chaperone properties rather than localization. The organellar categorization of ER or MITO specific represents chaperones for which the biochemical, genetic, and cell biological evidence supports both chaperone function and organellar-specific localization and for which no IPR domain match could be obtained.

Of the 332 genes that comprise the human chaperome, 88 are functionally classified as chaperones and 244 are co-chaperones. Among the 88 chaperones are 50 ATP-dependent chaperone genes and 38 ATP-independent chaperones. The ATP-dependent chaperones are comprised of the 5 HSP90s, 17 HSP70s, 14 HSP60s, 6 ER-specific, and 8 MITO-specific Hsp100/AAA+ ATPases, respectively. In the HSP70 family are the 17 holding and folding ATP-dependent HSP70s and ten ATP-independent co-chaperones, corresponding to the nucleotide exchange factors (NEFs) BAG1–BAG6, the GrpE NEFs GRPE1 and GRPE2, SIL1 (Hsp110/BAP), and HSPBP1 (Mayer, 2013). Likewise, the HSP90 family is comprised of 46 members including the five ATP-dependent HSP90 chaperones (Pearl and Prodromou, 2006) and 41 ATP-independent co-chaperones that regulate HSP90 including the two AHA1 co-chaperones (AHSA1 and AHSA2), CDC37, CDC37L1, p23, and 36 immunophilins subclassified into 18 cyclophilins and 18 FKBPs. The 49 HSP40s correspond to a separate family of ATP-independent co-chaperones that function as holding chaperones and HSP70 co-chaperones. Taken together, the HSP90, HSP70, and HSP60 chaperone systems correspond to 26.5% of the chaperome, with the HSP40s contributing another 15% to the chaperome.

Among the 38 ATP-independent chaperone genes are ten sHSPs, nine prefoldins, four MITO-specific, and 15 ER-specific chaperones. Another 19% of the chaperome are represented by the 48 ER-specific and 14 MITO-specific chaperones (Figure 1A; Table S2A) including 26 ER-specific oxidoreductases and two MITO-specific protein-disulfide-isomerase-type thioredoxins. Notably, the largest chaperome subclass is the 114 TPR domain-containing genes, representing 34% of the chaperome. These include STIP1 (HOP) that functions as an HSP70 and HSP90 co-chaperone (Prodromou et al., 1999; Song and Masison, 2005) and contains three TPR-classifier IPR domains (IPR001440, IPR013026, and IPR019734). Although many of these newly identified members of the TPR-domain family have not been yet shown to function as HSP70 and HSP90 co-chaperones, we opted for a comprehensive and inclusive approach. Some of these members have been recently validated in *C. elegans* using biochemical assays (Haslbeck et al., 2013). This organization into nine functional families lends itself to a systems-level evaluation of chaperome functionality in aging and disease.

Differential Chaperome Dynamics in Human Brain Aging

We examined the dynamics of the human chaperome using gene expression data from the superior frontal gyrus (SFG) of 48 brains from neuropathologically and neurologically normal control individuals of 20–99 years (Berchtold et al., 2008; Loerch et al., 2008). Analysis of the expression patterns of the human chaperome (Figure 1B) revealed a profile that correlated with aging ($p = 6.86 \times 10^{-6}$) and clustered into two groups with a mean age of 36 ± 4 years and 73 ± 4 years (Figures 1B and 1C). These age groups are highly pronounced upon hierarchical clustering but are discernable even when ordered by chronological age (Figure S1A).

Aging correlation analysis of the human chaperome expressed in the SFG identified 101 chaperone genes (31.8%) that are repressed ($corr_{age} < 0$ and $p < 0.05$), and 62 (19.5%) genes that are induced during aging ($corr_{age} > 0$ and $p < 0.05$; Figure 1B; Table S3). Chaperome age expression revealed enrichment of certain functional families in induction and repression clusters (Figures 1B and S3A–S3D). TPR proteins tend to be induced, whereas HSP40s are repressed (Figure 1B). The significance of the repression and induction clusters is further supported by analysis of an independent data set from frontal lobes of individuals of 24–40 years and 70–94 years (Loerch et al., 2008; Figure S1D). Clustering identified isochronal aging repression and induction clusters with a significant boundary between the two age groups (Figures 1B, 1C, S1A, and S1B). Analysis of both data sets revealed that the chaperome genes repressed and induced in both data sets of normal brain aging overlapped significantly ($p < 2.2 \times 10^{-16}$ and $p = 1.7 \times 10^{-12}$, respectively; Figures

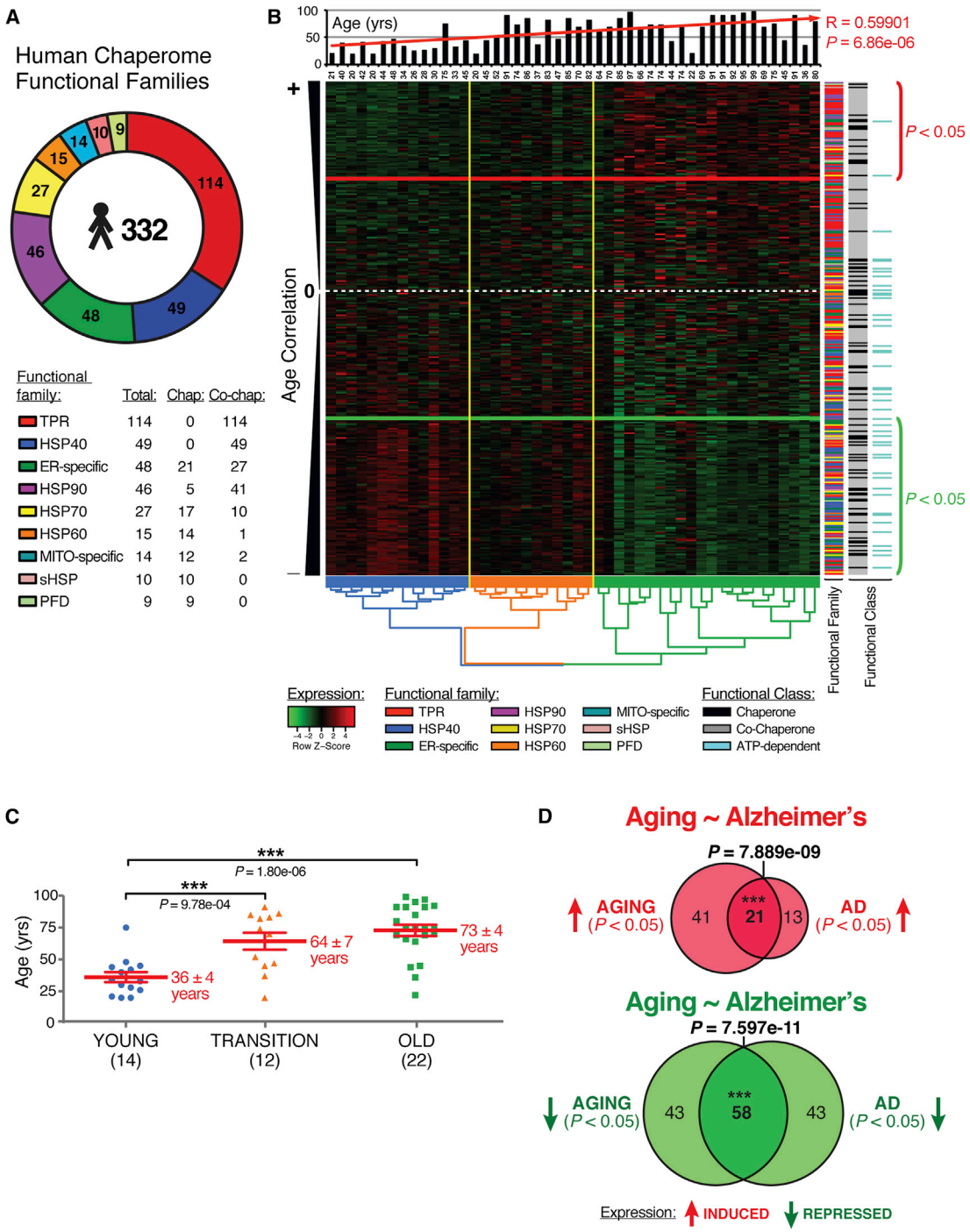

Figure 1. Differential Chaperome Responses in Human Brain Aging and Neurodegenerative Disease

(A) The human chaperome. Functional families and number of members are indicated.

(B) Heatmap showing 318 chaperones expressed in human brain (super frontal gyrus) ordered by decreasing age correlation. The white dashed line indicates age-expression correlation coefficient closest to zero. Genes above the red line are induced ($p < 0.05$); genes below the green line are repressed ($p < 0.05$). The histogram visualizes specimen age upon hierarchical clustering. The dendrogram visualizes hierarchical clustering of brain specimens. The y axis color code highlights from left to right the nine chaperome families, chaperones (black), co-chaperone (gray), and ATP-dependent chaperones (turquoise).

(C) Three major age groups (blue, "young"; orange, "transition"; green, "old") are visualized by dendrogram coloring in (B). Values are mean age ± SEM. ***$p < 0.001$; Student's t test.

(D) Overlaps of chaperones induced (red) or repressed (green) in aging versus AD.

See Figures S1–S3.

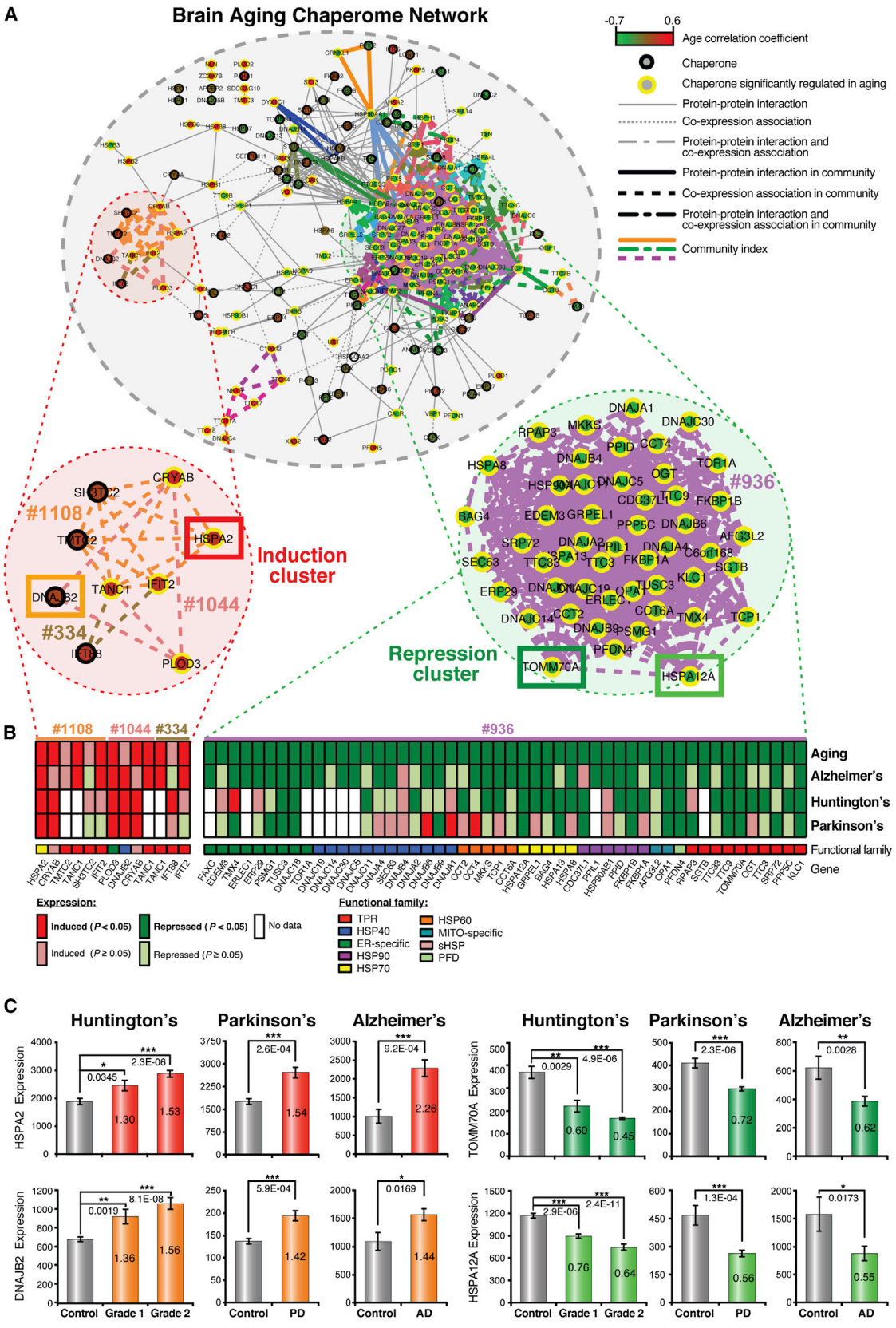

(legend on next page)

S1E and S1F). We observed similar age clusters with significant boundaries in entorhinal cortex (Figure S1C), confirming chaperone expression dynamics in brain aging in different data sets.

Concordant Dynamics of Chaperome Expression in Brain Aging and Neurodegenerative Diseases

Because aging represents a risk factor for neurodegenerative disease, we assessed the impact of AD, HD, and PD on chaperome dynamics by examining expression in patient brain samples (Hodges et al., 2006; Moran et al., 2006; Liang et al., 2008; Table S3C–S3E). When analyzing brain-expression data sets from AD patients, we identified 101 significantly repressed genes and 34 induced genes compared to age-matched controls. Both in aging and AD brains, chaperome repression is significantly enriched compared to overall gene repression in the genome (Figures S2A and S2B). We then asked whether the chaperome genes differentially regulated in AD overlapped with the aging-regulated chaperome genes and identified 21 genes that overlapped between the 62 genes induced in aging and 34 genes induced in AD ($p = 7.89 \times 10^{-9}$) and 58 genes that overlapped between 101 aging-repressed and 101 AD-repressed chaperone genes ($p = 7.6 \times 10^{-11}$; Figure 1D). Among the genes that are repressed in both aging and AD, the HSP70-HSP40 system corresponds to 36% of the 58 genes (Table S3D). Chaperome genes consistently repressed in aging and AD include members of all nine functional chaperome families, revealing that alterations in chaperone expression are not selective to specific gene families. The 21 genes induced in both aging and AD extend across all functional families except HSP60 genes. Similarly, we also examined whether the chaperome genes regulated in aging overlapped with those dynamically regulated in HD and PD. Among the 245 chaperome genes detected in all data sets, 36 genes overlapped between genes repressed in aging and HD ($p = 3.96 \times 10^{-7}$) and 24 genes between aging and PD ($p = 0.01062$; Figures S2C and S2E). Chaperome genes induced in aging also significantly overlapped with genes induced in HD ($p = 2.94 \times 10^{-10}$) and PD ($p = 0.00059$; Figures S2D and S2F; Table S3).

We partitioned the chaperome age-expression distribution into the nine families and observed reproducible expression patterns in four distinct brain tissues (Figures S3A–S3D). Ranked by decreasing median aging correlation, the induction of sHSPs and TPR genes consistently ranked high and the HSP60s, HSP40s, and HSP70s were consistently repressed. Among repressed genes, the HSP40s exhibited significant change ($p = 0.04875$), with 62% of 48 HSP40 genes repressed in aging ($p < 0.05$) and 51% repressed in AD. Of these, 41% are repressed in both aging (SFG) and AD ($p = 0.0009$). Among the genes that are induced in brain aging and disease are sHSPs and TPR-containing chaperone genes (Figures S3A–S3D).

The distribution of ATP-dependent chaperones in aging and AD was shown to be enriched 10-fold in the repression cluster of aging SFG ($p = 4.8 \times 10^{-6}$) and 11-fold in the prefrontal cortex (PFC) ($p = 1.7 \times 10^{-7}$; Figure S3E) whereas ATP-independent chaperones exhibited equivalent levels of repression and induction. This analysis of the chaperome in human brain aging also reveals concordant exacerbation of responses in neurodegenerative disease. These concordant chaperome changes provide evidence for significant changes in the proteostasis network in aging and neurodegenerative disease.

Chaperome Network Community Dynamics in Brain Aging and Disease

The repression and induction of chaperones in brain aging likely affect the cellular balance of chaperone machines and functionality of the PN, leading us to consider how these components of the chaperome are physically and functionally associated. We visualized the systems-level connectivity of the chaperome by integrating physical protein-protein interactions (PPI edges) from public databases together with coexpression pairs in aging brains (COX edges; Tables S4 and S5) into a PPI-COX interactome (Figure 2A). The COX edges were identified using transcriptome data from SFG tissue given its highly significant and pronounced aging dynamics. Among all 50,403 chaperome pairs, we found 1,193 significant COX edges ($corr_{age} > 0.8$ and $p < 0.05$), of which 15 of 191 unique PPIs are also COX edges. Applying the link-community-clustering algorithm (Ahn et al., 2010) to the PPI-COX network, we identified 40 link communities, of which 34 are repression communities compared to only six induction communities (Figure 2A; Table S6).

This network community-clustering analysis also revealed that the majority of genes residing in induction or repression link communities showed concordant patterns in aging and neurodegenerative diseases, respectively (Figures 2A and 2B), leading to the hypothesis that these aging-expression changes can affect the cellular balance of chaperone machines and functionality of the PN. For example, concordantly aggravated expression patterns for the aging-induced genes HSPA2 (HSP70) and DNAJB2 (HSP40) and the aging-repressed HSPA12A (HSP70) and TOMM70A (TPR) were observed in brain biopsies from AD, HD, and PD patients (Figure 2C). In terms of gene-expression dynamics in aging and disease, these exemplary genes are representative for induction and repression cluster dynamics. Included in the repression cluster are members across eight of

Figure 2. Chaperome Network Community Dynamics in Brain Aging and Age-Onset Neurodegenerative Diseases

(A) Integrated human chaperome network based on physical protein-protein interaction (PPI) and coexpression (COX) edges and link communities of chaperones concordantly induced or repressed during brain aging. PPIs (solid edges). COX > 0.8 (dashed edges). Color scale indicates positive to negative correlation between age and gene expression. Link communities highlighted by edge color; yellow node borders indicate significant age-expression correlation ($p < 0.05$).

(B) Heatmaps visualize induction or repression in aging, AD, HD, and PD at node resolution for communities highlighted in (A). Community numbers and gene names are indicated. Color code micrographic visualizes functional family. Significantly induced and repressed genes ($p < 0.05$) shown in dark red and green, respectively, and nonsignificantly induced and repressed genes with $p \geq 0.05$ are shown in light red and light green. See Figures S2 and S3.

(C) Chaperones and co-chaperones selected from induction and repression communities and their expression in brains from AD, HD, and PD patients. Values are average expression ± SEM. Values indicated inside the bars indicate ratios of expression in disease over control. *$p < 0.05$; **$p < 0.01$; ***$p < 0.001$; Student's t test.

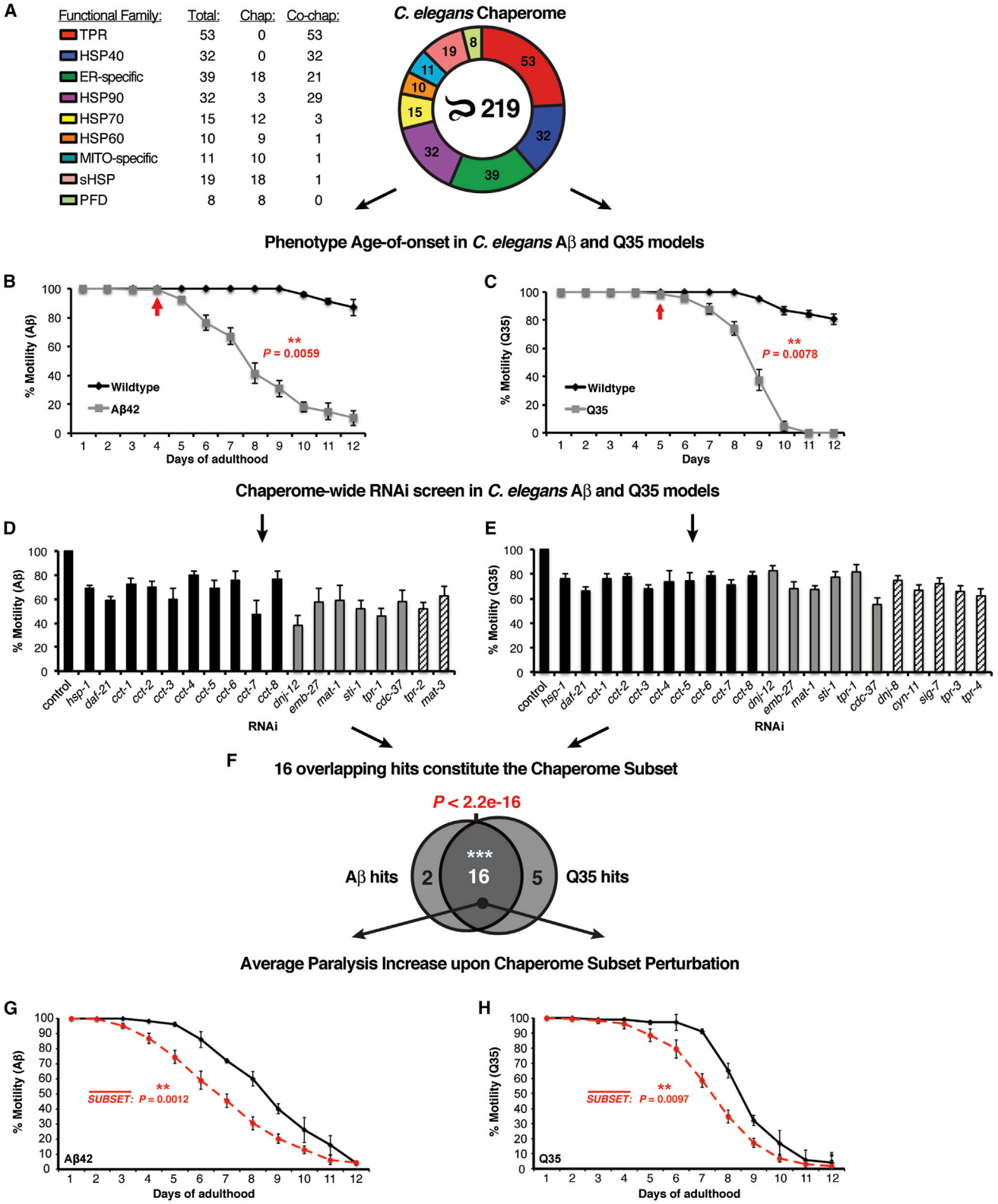

(legend on next page)

nine chaperone gene families with predominance of ATP-dependent chaperones and HSP40 co-chaperones, whereas induction communities are enriched for TPR-domain co-chaperones and sHSPs. These observations provide support that prominent changes in chaperone expression levels could accelerate AD, HD, or PD disease pathology characterized by elevated toxic gain-of-function aggregation. Chaperome repression communities dominate the network landscape in human brain aging and disease, linking known chaperones and co-chaperones with less well-characterized chaperones, possibly revealing novel interactions important for the aging and disease PN.

Chaperome Function in *C. elegans* Models of Protein Aggregation

To complement the bioinformatics analysis of the human chaperome with in vivo functional data, we experimentally validated the functional consequences of repressed chaperome gene expression and function during aging and disease using two established *C. elegans* models expressing the cytotoxic aggregation-prone proteins, Aβ ($A\beta_{42}$) and polyQ (Q35), implicated in AD and polyglutamine (HD) diseases, respectively (Link, 1995; Satyal et al., 2000; Morley et al., 2002). In both models, aggregation and toxicity, measured by decreased motility, increases in an age-dependent manner and can be suppressed by lifespan-enhancing pathways such as the insulin-like signaling pathway (*daf-2* and *age-1*) and the heat shock response (*hsf-1*; Morley et al., 2002; Cohen et al., 2006). We assembled and curated the *C. elegans* chaperome by orthology mapping and manual curation (Harris et al., 2010; Sayers et al., 2012; see Supplemental Experimental Procedures) and identified 219 *C. elegans* chaperone and co-chaperone genes, corresponding to the same nine functional gene families (Table S2B). Comparison of *C. elegans* and human chaperomes revealed similar proportions of most functional families, with notably a reduction in TPR domain co-chaperones to 24% of the *C. elegans* chaperome from 34% in the human chaperome and increased number of sHSPs to 19 genes in *C. elegans* from ten sHSP genes in humans (Figure 3A).

We first examined the functional requirements of all 219 *C. elegans* chaperome genes using RNAi knockdown in animals expressing $A\beta_{42}$ by monitoring early-onset paralysis on day 4 of adulthood (Figure 3B). Based on our methodology of screening, assessing age-dependent aggregation and toxicity phenotypes (measured by decreased motility), genes when knocked down that caused motility defects in both wild-type and disease models were eliminated; in other words, genes that gave the same magnitude of phenotypic change in wild-type animals were not further considered. This functional screen identified 18 genes (Figure 3D), corresponding to ten ATP-dependent chaperones, HSC70 (*hsp-1*), HSP90 (*daf-21*), and eight subunits of the CCT/TRiC chaperonin complex; the co-chaperones, HSP40 (*dnj-12*) and CDC37 (cdc-37); and the TPR-domain protein STI1 that upon knockdown significantly enhanced $A\beta_{42}$ proteotoxicity (Figure 3D). Included among these modifiers were four TPR-domain proteins; the anaphase-promoting complex (APC/C) subunits *mat-1*, *mat-3*, and *emb-27*; and the uncharacterized open reading frames, Y39A3CR.3 (*tpr-1*) and Y57G7A.10 (*tpr-2*), conserved in human as TTC7A/TTC7B and EMC2, with a phenotype on the $A\beta_{42}$ animals that were not previously implicated in proteostasis.

To test whether the chaperone genes that regulate $A\beta_{42}$ proteotoxicity have more general effects, we performed a subsequent RNAi screen using a *C. elegans* model for expression of aggregation-prone polyQ (Q35), associated with HD pathogenesis. This model of chronic Q35 protein expression and aggregation exhibits an early-onset, age-dependent decline in muscle function (Figure 3C; Morley et al., 2002). Knockdown of 21 of the 219 *C. elegans* chaperome genes significantly enhanced polyQ-dependent proteotoxicity (Figure 3E). These correspond to the same ATP-dependent chaperones (*daf-21*, *hsp-1*, and the eight CCT/TRiC complex subunits) that overlapped with the $A\beta_{42}$ screen and 11 co-chaperones, of which six genes were identified in both screens, including the TPR-domain APC/C subunits *mat-1* and *emb-27* and the TPR protein, Y39A3CR.3 (*tpr-1*; Figures 3D and 3E). These results reveal an overlapping common subset of 16 chaperome genes including the newly identified members of the APC/C ($p < 2.2 \times 10^{-16}$; Fisher's exact test; Figures 3D–3F). Additionally, these screens also identified seven chaperones with more selective phenotypes on either $A\beta_{42}$- or Q35-expressing animals.

To investigate whether the common chaperome subset also affects age-related proteotoxicity, we assessed the functionality of *C. elegans* muscle throughout adulthood (days 1–12) following RNAi knockdown of all 16 subset genes in both models. All 16 genes were highly protective in the $A\beta_{42}$ ($p = 0.0012$) and Q35 models ($p = 0.0097$) and showed significant reduction in motility upon RNAi, suggesting that repression of the chaperome subset

Figure 3. Functional Chaperome Perturbation Analyses in *C. elegans* Models of Protein Misfolding

(A) The *C. elegans* chaperome with its functional families and numbers of members per family are shown.

(B) Paralysis (% motility) for wild-type and $A\beta_{42}$-expressing *C. elegans* from day 1 to day 12 of adulthood. Arrow indicates paralysis age of onset. Data points are average percent motility ± SEM ($n = 3$ and $n \geq 25$ animals/trial). **$p < 0.01$; Student's t test.

(C) Motility defects for wild-type and Q35-expressing *C. elegans* from day 1 to day 12. Arrow indicates age of onset. Data points as in (B).

(D) RNAi paralysis phenotypes on day 4 of adulthood (% motility) for *C. elegans* expressing $A\beta_{42}$ (mean ± SEM; $n = 3$ and $n \geq 25$ animals/trial). Values are average percent motility ± SEM ($n = 3$ and $n \geq 25$ animals/trial).

(E) RNAi motility defects on day 2 of adulthood (% motility) for *C. elegans* expressing Q35 (mean ± SEM; $n = 3$ and $n \geq 25$ animals/trial). Values as in (D).

(F) Venn diagram indicating significant overlap of 16 hits from both screens ($p < 2.2 \times 10^{-16}$; Fisher's exact test).

(G) Average paralysis (% motility) for RNAi of all 16 chaperome subset genes in $A\beta_{42}$-expressing *C. elegans* throughout adulthood (days 1–12). Data points are averages of corresponding data points in each RNAi experiment ± SEM, each based on $n \geq 3$ independent experiments and $n \geq 25$ animals/trial. **$p < 0.01$; Student's t test.

(H) Average paralysis (% motility) for chaperome subset RNAi in Q35-expressing *C. elegans* throughout adulthood (days 1–12). Data points as in (G).

See Figure S4.

renders aged organisms more susceptible to proteotoxicity (Figures 3G, 3H, and S4).

A Chaperome Subset Safeguards Proteostasis in Aging *C. elegans*

Our network analysis of chaperome repression demonstrated concordant changes in brain aging and neurodegenerative disease (Figures 1D and S2). This led us to speculate whether expression of these chaperones also changes during aging, thus affecting the susceptibility of $A\beta_{42}$- and Q35-expressing animals to proteotoxic insult (Figures 3G and 3H). To address this, we monitored the age-dependent changes in motility of *C. elegans* that express a metastable temperature-sensitive mutation in paramyosin (UNC-15^{TS}) that misfolds in early adulthood at the permissive temperature (Gidalevitz et al., 2006). At the permissive temperature, knockdown of the chaperome subset (Figures 4A and S4C) substantially exacerbated the loss of muscle cell function during aging of UNC-15^{TS} animals, providing direct functional evidence for a protective role in aging.

To further characterize the chaperome subset during aging, we monitored various physiological phenotypes in wild-type and RNAi-treated animals and showed that this subset of the chaperome is important to prevent or delay age-dependent paralysis (Figures 4B, 4C, and S4D). Knockdown of *daf-21* (HSP90) or *hsp-1* (HSC70) led to increased paralysis in 45% and 44% of day 6 animals, respectively, and knockdown of TPR co-chaperones *tpr-1* and *dnj-12* resulted in 70% impairment (Figure S4D). The loss of motility in wild-type animals was due to deterioration of myofilament structure (sarcopenia). We monitored the integrity of MYO-3, a heavy chain component of myofilaments by MYO-3::GFP fluorescence and, upon knockdown of *dnj-12* and *emb-27*, observed more-severe sarcopenia at day 8 compared to day 1, whereas structural integrity of muscle was maintained up to day 8 in controls (Figure 4D). Consistent with these observations, RNAi of *cct-1*, *hsp-1*, and *daf-21* leads to premature Q35 aggregation (Figure 4E), recapitulating the misfolding of disease-associated polyQ proteins, a hallmark of HD. Our evidence at cellular and organismal levels suggests that the chaperome subset safeguards proteostasis during aging.

The Chaperome Subset Safeguards Proteostasis in Human Cells

To test whether the chaperome subset identified in *C. elegans* models of Aβ and Q35 proteotoxicity functionally extends to the human chaperome, and to test its potential contribution to HD, we used a high-content imaging assay to quantify aggregation of doxycycline-inducible Huntingtin-exon1(Q78)-GFP (Htt-GFP) expressed in HeLa cells. The 16 subset *C. elegans* chaperones and co-chaperones correspond to 28 genes in the human genome, of which 24 genes are expressed in HeLa cells (Nagaraj et al., 2011; Figure 5A). We confirmed small interfering RNA (siRNA) knockdown efficiency of HTT-GFP, CCT2, DNAJA1, and HSPA8 by immunoblot analysis to show reduced levels of these chaperones (Figure S5A). An increase in the fraction of Htt-GFP-expressing cells with protein aggregates was observed upon knockdown of 15 human chaperones compared to control, corresponding to 63% of the human chaperome subset and 75% of the worm chaperome subset, respectively (Figure 5B; Table S7). These included all subunits of the CCT/TRiC complex (except CCT5); HSP40 and HSP70 family members DNAJA1 (HDJ-2), DNAJA4, HSPA8 (HSC70), and HSPA14 (Figures 5B and 5C); and the TPR-domain APC/C subunits CDC23 and CDC27 that, upon knockdown, led to significantly elevated aggregation (Figure S5B). The overall protective effect of the chaperome subset in human cells against Htt-GFP aggregation provides additional functional evidence to support the results from the *C. elegans* RNAi analysis of the chaperome subset in proteotoxicity.

The Chaperome Subnetwork Is Repressed in Brain Aging and Disease

Whereas broad chaperome repression in aging human brains pointed toward proteostasis functional decline and increased susceptibility to proteotoxic insults in neurodegenerative diseases, our functional screens in *C. elegans* led to the identification of a common chaperome subset. To investigate the dynamics of the corresponding chaperome subset in human brain aging and disease, we examined the connectivity of the chaperome interactome and partitioning across communities of induction and repression. We matched orthologous human chaperome subset nodes in the PPI-COX chaperome interactome to visualize their expression dynamics and interactome topology (Figure 6A). Of the 28 human nodes, 27 genes are expressed in the human brain (Berchtold et al., 2008), of which the majority (20 genes) are interconnected in a major component involving 60 edges. This human chaperome subnetwork is significantly interconnected ($p < 0.01$; Figures 6A and S6A–S6C). The subnetwork nodes include five chaperone families and have a higher degree of connectivity than nonsubnetwork nodes ($p = 0.04$; Figure S6D). Overall, 52% of subnetwork nodes are repressed in aging brain compared to 30% repression of nonsubnetwork nodes ($p = 0.0292$; Fisher's exact test; Figure 6C). Likewise, 52% of subnetwork nodes are significantly repressed in AD compared to 30% repression of nonsubnetwork nodes ($p = 0.0292$; Fisher's exact test), 24% in HD, and 16% in both diseases (Figure 6C). The chaperome subnetwork is nearly 2-fold more repressed in brain aging and AD as opposed to nonsubnetwork chaperome genes. We further tested the significance of the overlaps of subnetwork genes repressed in all conditions, aging, AD, and HD as compared to nonsubnetwork genes, asking whether the subset of chaperome subnetwork genes repressed in both AD and HD is significantly enriched. Four genes that are significantly repressed both in AD and HD (HSP90AB1, HSPA8, HSPA14, and TCP1) are also repressed in aging (Figure 6B). We applied a Fisher exact test considering all chaperome genes significantly repressed in at least one condition, AD, HD, or aging, which includes 19 chaperome subnetwork and 142 nonsubnetwork chaperome genes. The significance of the observation that a set of four genes repressed in AD and HD is also repressed in aging ($p < 10 \times 10^{-5}$; Fisher's exact test; Figure 6D) demonstrates the power of integrating data from more than one disease and aging. Some of the subnetwork chaperome nodes that were not significantly repressed in aging are repressed in AD, including the APC/C complex TPR-domain subunits

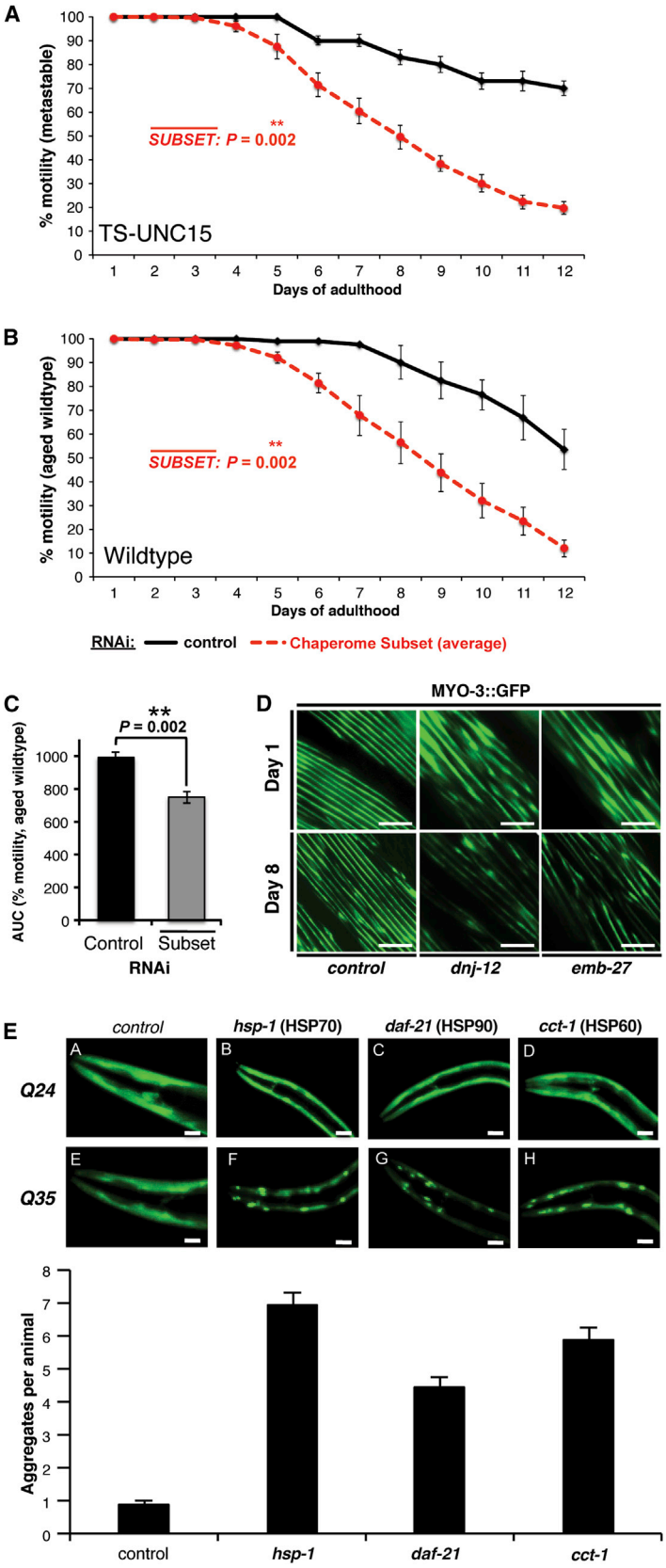

Figure 4. A Chaperome Subset Safeguards *C. elegans* Proteostasis against Aging-Related Proteotoxicity

(A) Average paralysis (% motility) for chaperome subset RNAi in the *unc-15*(*e1402*) TS strain at 15°C throughout adulthood (days 1–12). Data points are averages of corresponding data points in each RNAi experiment ± SEM, based on n ≥ 3 experiments and n ≥ 20 animals/trial. **p < 0.01; Student's t test.

(B) Average paralysis (% motility) in aged wild-type animals throughout adulthood (days 1–12). Data points as in (A).

(C) Early-onset paralysis (% motility) upon chaperome subset RNAi in aged wild-type animals (compare B) as area under the curve (AUC) for control aging wild-type worms (average ± SEM; n = 5) and average of RNAi-treated aging wild-type worms (average of 16 subset phenotypes ± SEM, each n = 3). **p < 0.01; Student's t test.

(D) Sarcopenia phenotype upon control, *dnj-12*, and *emb-27* RNAi visualized by MYO3::GFP fluorescence at day 1 versus day 8 of adulthood. The scale bar represents 10 μm.

(E) Early-onset aggregation of polyQ (Q35) expressed in body wall muscle cells upon chaperome subset RNAi. Q25, subthreshold polyQ. Graph shows increased average aggregate count upon RNAi compared to control ± SEM (n ≥ 100 animals; n = 3). The scale bar represents 0.02 mm.

See Figure S4.

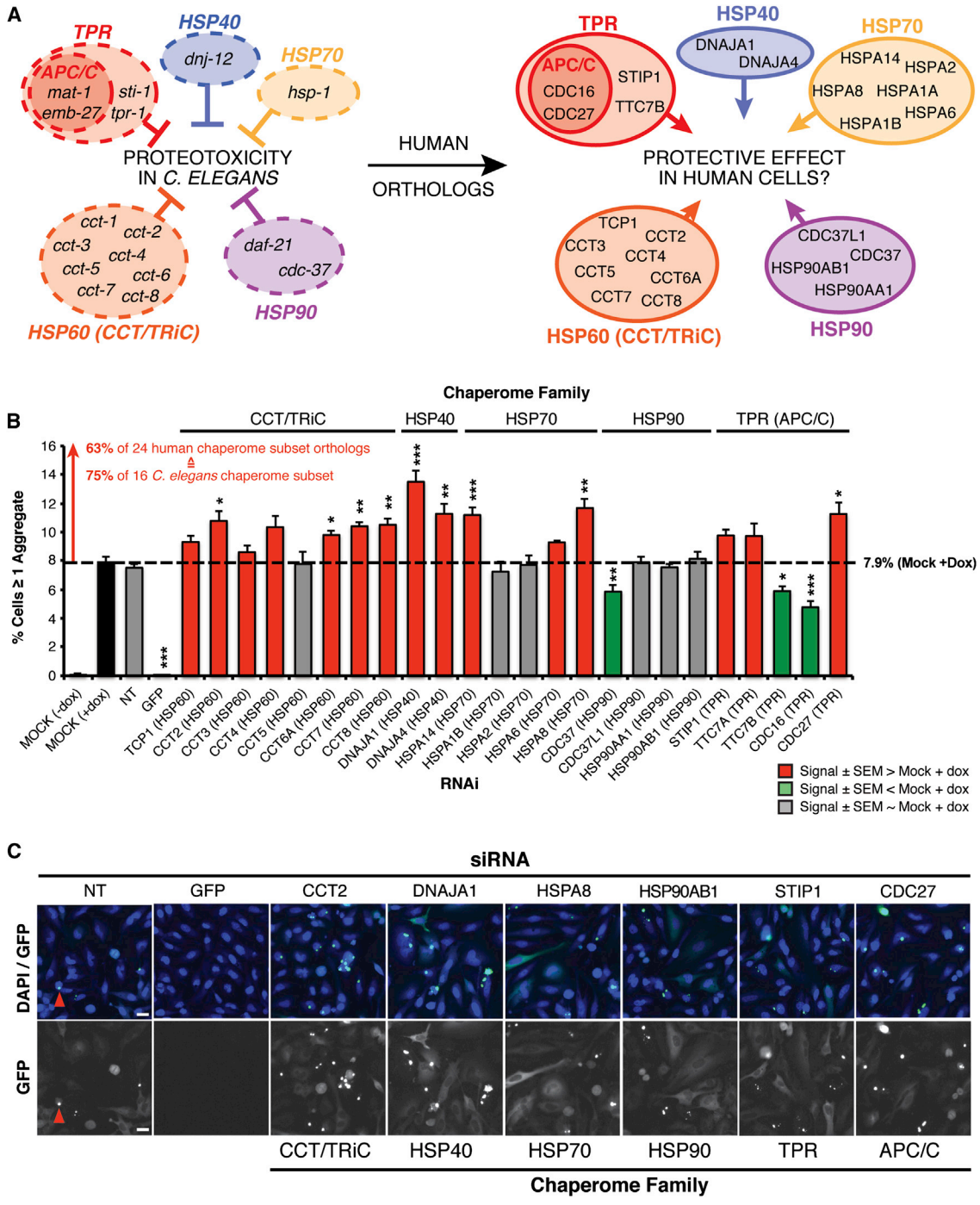

Figure 5. Human Chaperome Subnetwork Safeguards Proteostasis against Huntingtin Aggregation

(A) Sixteen chaperome subset members identified by RNAi screens in $A\beta_{42}$ and Q35 *C. elegans* models grouped by functional family. APC/C, anaphase-promoting complex/cyclosome and the corresponding 24 human chaperome subset members identified by orthology mapping.

(B) Percentage of HeLa cells with greater than or equal to one Huntingtin-exon1(Q78)-GFP (HTT-GFP) aggregate and upon siRNA. Results shown for all 24 human orthologs expressed in HeLa, corresponding to the 16 *C. elegans* chaperome subset members. Values are averages ± SEM (n = 6). Red, gray, and green bars represent increased, unchanged, and decreased aggregation, respectively, measured as "%Cells ≥ 1 aggregate". *p < 0.05; **p < 0.01; ***p < 0.001; Student's t test.

(C) Representative images for nontargeting (NT) siRNA, siRNA-GFP (positive control), and siRNA against each one member of the chaperome subset functional families are shown. Red arrows exemplify HTT-GFP aggregates. The scale bar represents 20 μm.

See Figure S5.

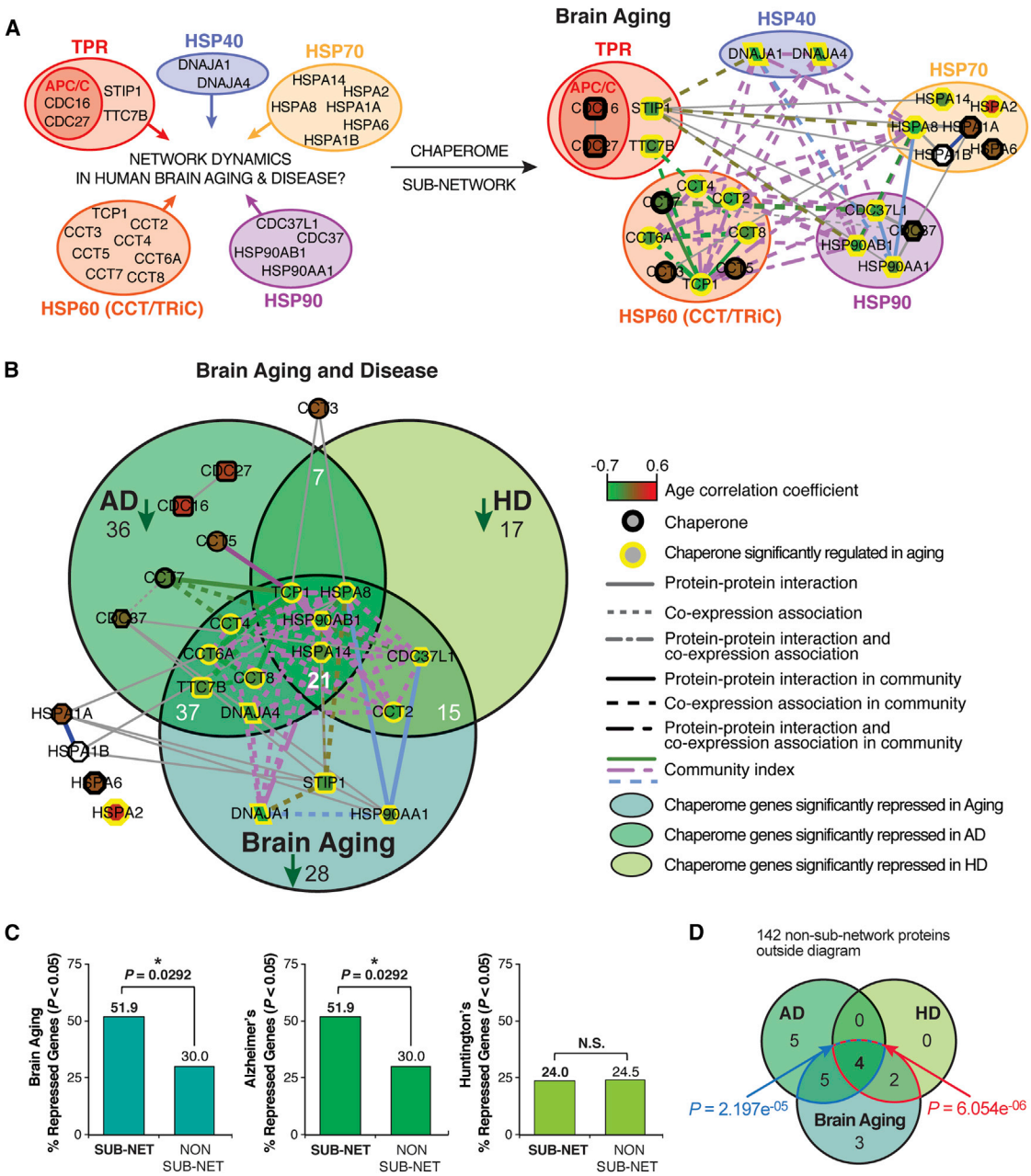

Figure 6. The Human Chaperome Subnetwork Is Repressed in Aging and Disease

(A) Extraction of the human orthologous chaperome subnetwork from the chaperome interactome shown in Figure 2A to highlight chaperome subnetwork dynamics in human aging brain and neurodegenerative disease. Nodes, edges, shapes, and edge strengths as in Figure 2A.

(B) Human chaperome subnetwork superimposed on Venn overlaps of chaperome genes significantly repressed in aging, AD, and HD.

(C) Graphs show percent subnetwork (sub-net) versus percent nonsubnetwork (non sub-net) chaperome nodes repressed in human aging brain (SFG) and brains from Alzheimer's (SFG) and Huntington's disease (PFC) patients (see Figure S6). SFG, superior frontal gyrus; PFC, prefrontal cortex.

(D) Venn diagram of overlaps of chaperome subnetwork genes significantly repressed in both AD and HD as well as in aging. p values are based on Fisher's exact test, considering only chaperones that are significantly repressed in at least one of the three conditions: aging, AD, or HD. The blue overlap area and p value indicate the significance of the overlap of subnetwork genes repressed in all three conditions against the union of subnetwork genes repressed in "aging only" and in "aging and AD"; the red overlap area and p value indicate the significance of the overlap of subnetwork genes repressed in all three conditions against the union of subnetwork genes repressed in aging only and in "aging and HD".

CDC16 and CDC27. These results reveal that the chaperome subnetwork is significantly more interconnected in the human interactome and concordantly more repressed in brain aging. The significantly enriched fraction of aging-repressed subnetwork chaperome nodes versus nonsubnetwork nodes and their aggravated repression in aging and disease is in agreement with

the chaperome subnetwork phenotypes observed in our RNAi functional perturbation experiments.

Thus, our orthogonally integrated chaperome-scale approach successfully identified a small subset of chaperones and specific co-chaperones from hundreds of chaperone and co-chaperone factors, including well-established and novel regulators of proteostasis maintenance in aging and disease that are highly interconnected in a chaperome subnetwork.

DISCUSSION

Molecular chaperones, being among the most highly conserved genes with essential functions for protein biogenesis, might have been thought to be equally important for proteome maintenance. Our analysis of chaperome dynamics combines the analysis of expression in human brain and neurodegenerative disease, experimental validation using *C. elegans* and human cells expressing disease-associated aggregates, and protein-protein interaction network analysis, from which we have identified a chaperome subnetwork affected in aging and disease. This study has identified a subset of the chaperome that is critical to maintain proteostasis in aging and upon challenge with neurodegenerative disease-associated proteins. This combined approach led to identification of a conserved subset of 16 genes in *C. elegans*, comprised of the ATP-dependent chaperones HSC70 and HSP90; the CCT/TRiC complex; and select HSP40 and TPR-domain co-chaperones that exhibit altered expression during human brain aging and are functionally required in *C. elegans* models to prevent proteotoxicity of neurodegenerative-disease-associated proteins. Of the human chaperome of 332 genes, 32% are repressed in brain aging, corresponding mostly to ATP-dependent chaperone machines involved in holding intermediates and folding to the native states, and are represented by highly connected repression clusters that concordantly decline in brains of AD, PD, and HD patients. We propose that changes in expression of the subnetwork may signify early events, leading to age-associated proteostasis collapse with implications for the pathogenesis of neurodegenerative disease.

The composition of the chaperome subnetwork highlights the central importance of specific ATP-dependent cytoplasmic chaperone machines during aging from *C. elegans* to human essential to achieve a healthy-tissue proteostatic state that can withstand challenge by expression of cytoplasmic polyQ expansion proteins or Aβ. Some of these chaperones such as the HSP70-HSP40 machine have been previously implicated in the modulation of polyQ-expanded protein aggregation (Cummings et al., 1998; Jana et al., 2000). Likewise, the level of cytosolic chaperonin affects polyQ toxicity by actively modulating the aggregation state, a major cause of polyQ cytotoxicity in Huntington's disease (Nollen et al., 2004; Behrends et al., 2006; Kitamura et al., 2006; Tam et al., 2006). Differences are revealed that may point toward aging or disease-specific subnetwork modules or contribution of only parts of the subnetwork to pathways involved in molecular pathology of these diseases. Notably, HSP90 resides at the intersection of aging, AD, and HD. The lower overall number of subnetwork versus nonsubnetwork genes repressed in HD compared to those repressed in AD could correspond to differences in the molecular underpinnings of these diseases, whereas the six subnetwork genes significantly repressed in HD are also significantly repressed in aging, including HSP90, HSP70, and chaperonin (TCP1), representative of the core cytoplasmic molecular folding machineries. In addition to identification of the major ATP-dependent chaperones in our functional screens, we show that components of the APC, an E3 ubiquitin ligase that targets proteins for degradation, are highly effective modifiers of Aβ and polyQ proteotoxicity phenotypes. Despite its established role in the exit from mitosis, it has been shown that the APC is functional in postmitotic neurons (Gieffers et al., 1999; Kim et al., 2009; Marrocco et al., 2009) with a role in cognitive processes (Kuczera et al., 2011). Further evidence suggests that deregulated APC function is associated with neurodegeneration and cognitive decline (Almeida et al., 2005; Li et al., 2008; Maestre et al., 2008), and a screen in yeast identified the APC as modifier of polyQ toxicity (Bocharova et al., 2008). Considering existing evidence, we propose that these APC components represent novel proteostasis modifiers with a role in degradation through their E3 ubiquitin ligase function, whereas mechanistically, it is possible that they may function as co-chaperones. Previous studies using RNAi in *C. elegans* have identified components acting in protein degradation as modifiers of polyQ proteotoxicity (Nollen et al., 2004).

The largest chaperome gene class is the 114 TPR-domain-containing proteins corresponding to 53 orthologs in *C. elegans*, accommodating, in an unbiased way, the large degree of functional heterogeneity of TPR-domain proteins in chaperone-related function. Four *C. elegans* proteins contribute to the chaperome subnetwork (*sti-1*, *mat-1*, *emb-27*, and *tpr-1*), and another four were identified to affect proteostasis in the Aβ (*tpr-2* and *mat-3*) and polyQ (*tpr-3* and *tpr-4*) models, of which none except *sti-1* had been previously described to have a role in proteostasis. The TPR family contains the largest number of members that have not yet been shown to function as HSP90 and HSP70 co-chaperones, although a recent biochemical analysis in *C. elegans* identified 13 TPR proteins that interact with HSP70 or HSP90 (Haslbeck et al., 2013). Based on our inclusive and unbiased chaperome-scale in vivo results from two independent screens, we identified additional TPR-domain proteins to be functionally equivalent to HSP90 or HSC70, leading us to propose that these factors harbor properties that are highly linked to proteostasis network maintenance and concordantly regulated with global chaperome dynamics in aging and disease.

Previous efforts to characterize chaperone networks have proposed subnetworks that participate in the folding of newly synthesized proteins and those that interact with preexisting proteins that become denatured upon acute stress (Albanèse et al., 2006). Our network analysis combines chaperome-expression analysis in aging brains with community network clustering to organize the connectivity dynamics of the human chaperome network and provides a 3D representation of the chaperome subnetwork within the context of the complete chaperome interactome. The subnetwork nodes are more interconnected and repressed than nonsubnetwork chaperome nodes and suggests that perturbation of a subnetwork node and its edges would result in a more severe perturbation of network integrity compared to the more peripheral low-degree

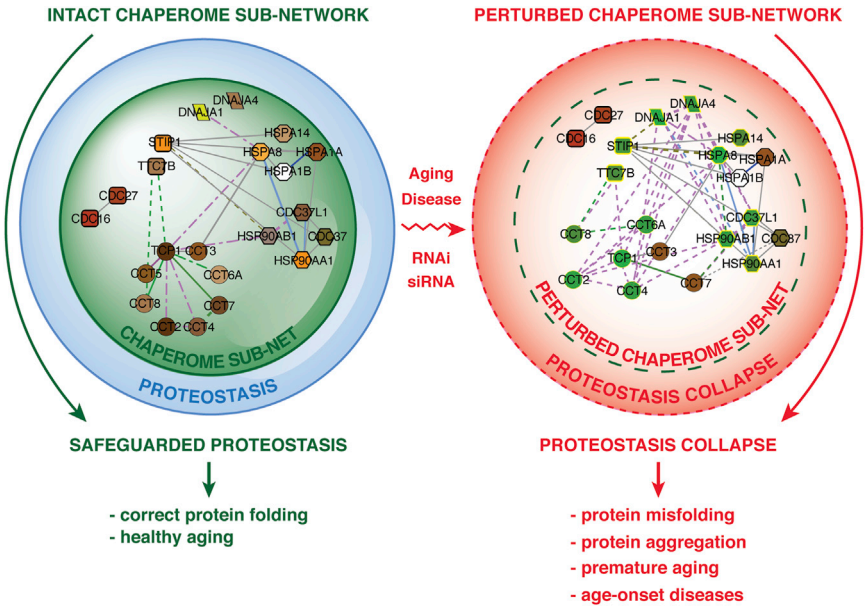

Figure 7. The Chaperome Subnetwork as Proteostasis Safeguard and Its Collapse in Disease

(A) Chaperome subnetwork action as buffer that safeguards proteostasis from proteotoxic stress, facilitating healthy development and aging.

(B) Chaperome subnetwork perturbation entails proteostasis collapse, exposure to proteotoxicity, accelerated aging, and age-onset disease. Perturbation exemplified by loss of edges and repression of gene expression (green nodes).

nonsubnetwork nodes. Accordingly, loss of protective chaperome subnetwork buffering capacity compromises proteostasis capacity, leading to an increased sensitivity to endogenous and exogenous stress and disease predisposition (Figure 7).

The HSP90 chaperone has been proposed to have buffering capacity in its role as a capacitor of morphological variation and facilitator of evolution. Reduction of HSP90 levels below a critical threshold exposes cryptic endogenous variants such as genetic mutations that would otherwise be corrected or suppressed by HSP90 (Rutherford and Lindquist, 1998; Queitsch et al., 2002). Local fluctuations in the expression of HSP90 in one tissue are recognized by transcellular chaperone signaling by the compensatory expression of chaperones in distant tissues to achieve organismal proteostasis (van Oosten-Hawle et al., 2013). The chaperome subset described here unites HSP90 and its co-chaperones with several novel and previously undescribed PN components in a highly interconnected subnetwork. We propose that the chaperome subnetwork, rather than individual chaperones, is important for the properties of the PN in aging and disease and suggest that this subnetwork is a functional "core chaperome" within the global chaperome (Powers and Balch, 2013). Based on the importance of proteostasis in health and disease, we suggest that chaperome subnetwork-targeted therapeutic interventions may be beneficial for a large number of age-related protein-misfolding disorders (Powers et al., 2009).

EXPERIMENTAL PROCEDURES

Chaperome Gene List Curation, Annotation, and Orthology Mapping

We curated the literature for chaperone and co-chaperone families, covering all structural and functional categories and subcellular localizations relevant to chaperone-assisted protein folding, and comprehensively annotated the human and *C. elegans* family members. We matched genes with domain structures referenced in UniProt, prioritizing 44 bona fide IPR-criteria domains (IPR-IDs) (Table S1) characteristic of each family to consolidate our literature-based annotation and to identify members not previously associated with these families. We organized the genes into nine functional families based on literature evidence on activities and the IPR-criteria domains. Chaperones with exclusive function in the ER and MITO compartments for which no IPR domain could be matched were grouped as "ER-specific" and "MITO-specific". Small co-chaperone families with unambiguous functional association with a chaperone were grouped within the respective chaperone system (family). HSP40 and TPR-domain co-chaperones were organized in separate families. Human and *C. elegans* chaperome gene lists were matched and reconciled using orthology pairs with the National Center for Biotechnology Information (NCBI) HomoloGene database. The annotations were recurated based on the WormBase (release WS234) comparative genomics tool that associates *C. elegans* genes with human orthologs based on curated and automated predictions by NCBI KOGs, InParanoid, TreeFam, precomputed BLAST results, Ensembl COMPARA, and the orthologs matrix project (OMA). We applied bipartite mapping to identify orthology pairs and the respective species-specific chaperome subsets.

Chaperome Expression Correlation Analyses

Expression profiles for 318 human chaperome genes were extracted from two independent transcriptome data sets of human brain biopsy tissue samples, covering subjects from a variety of ages (Berchtold et al., 2008; Loerch et al., 2008). We calculated Pearson correlation between age and each chaperone's expression and evaluated significance of correlation ($p < 0.05$). Hierarchical clustering was performed to cluster samples by expression profile similarity. For further details, see Supplemental Experimental Procedures.

Construction of the Integrated Brain-Aging Chaperome Interactome

We retrieved 64,738 unique human PPIs from MINT, BioGRID, HPRD, and IntACT and extracted the human chaperome interactome. Among these, we identified PPIs involving chaperome genes expressed in superior frontal gyrus of aging human brains (Berchtold et al., 2008). Coexpression correlation coefficients ($corr_{age}$) were calculated for all-by-all gene pairs to identify pairs with significant Pearson correlation of coexpression. Pairs with $corr_{age} \geq 0.8$ ($p < 9.0 \times 10^{-12}$) were considered significantly coexpressed (COX) and combined with PPIs into an integrated PPI-COX network. Visualizations were generated in Cytoscape v2.8.1 (Smoot et al., 2011).

Chaperome Network Community Clustering

We applied the link-community-network-clustering algorithm gauged at a community size cutoff of greater than or equal to three nodes and greater than or equal to two edges (Ahn et al., 2010) to identify communities of interconnected aging-coregulated chaperome genes. See Supplemental Experimental Procedures.

C. elegans Strains and Maintenance

C. elegans wild-type Bristol strain N2, $A\beta_{42}$ CL2006 (*dvIs2*), Q35 AM140 (*rmIs132*[*Punc-54*::*q35*::*yfp*]), the temperature-sensitive (TS) mutant strain

CB1402 (*unc-15*(*e1402*)), and the RW1596 (*myo-3*(*st386*);*stEx30*[*myo-3*::*GFP*;*rol-6*(*su1006*)]) strains were maintained according to standard methods at 20°C on nematode growth media with OP50 *E. coli* (Brenner, 1974).

C. elegans RNAi Screens for Chaperome Modifiers of Protein-Misfolding-Related Proteotoxicity

Chaperome-wide RNAi screens for enhancement of motility defects in *C. elegans* body wall muscle cells were performed using the commercial RNAi library. Missing or incorrect clones were cloned into L4440 (Kamath and Ahringer, 2003). Synchronized L1 animals expressing $A\beta_{42}$ or polyQ were fed bacteria expressing RNAi for each target. In case of lethality or larval arrest, worms were fed at the L4 stage. Adult worms from age-synchronized populations were scored for paralysis (Link, 1995; $A\beta_{42}$ screen) on day 4 or for motility defects (Silva et al., 2011; Q35 screen) on day 2 of adulthood. RNAi candidates with 20% decrease in movement compared to control in greater than or equal to three experiments constitute the final set. For aging-related proteotoxicity, synchronized adult animals fed chaperome subset RNAi were assayed daily, and nonresponders to prodding were scored as paralyzed. *unc-15*(*e1402*) animals were grown at 15°C and assayed daily for paralysis. To assess myofilament structure, we monitored MYO-3::GFP fluorescence in animals fed bacteria expressing double-stranded RNA against each target. Images were taken on days 1 and 8 of adulthood using a Zeiss Axiovert 200 microscope. See Supplemental Experimental Procedures.

Human Chaperome Subnetwork Interactome

We extracted 28 human orthologs of the 16 chaperome subset genes as described. The human chaperome subnetwork was obtained as a subnetwork of the PPI-COX chaperome interactome. To test significance, we built 100 randomized control PPI-COX networks, keeping number of nodes, edges, and node degree constant but rewiring edges between nodes and treating PPI and COX edges separately to conform to the different nature of these interactions. Network figures were generated with Cytoscape.

siRNA-HCI for Modifiers of Huntingtin Aggregation

Chaperome modifiers of Htt-GFP aggregation (percent of cells greater than or equal to one aggregate) were identified by siRNA perturbation coupled to high-content imaging (HCI) in HeLa cells. Monoclonal doxycycline-inducible cells expressing Htt-GFP were transfected with nontargeting or quadruplex siRNA smart pools. Cells were fixed, stained with Hoechst dye, and analyzed. See Supplemental Experimental Procedures.

SUPPLEMENTAL INFORMATION

Supplemental Information includes Supplemental Experimental Procedures, six figures, and seven tables and can be found with this article online at http://dx.doi.org/10.1016/j.celrep.2014.09.042.

AUTHOR CONTRIBUTIONS

M.B., C.V., J.H.S., and A.V. performed experiments or contributed new reagents. M.B., T.R., S.W., Y.Z., and K.O. performed computational analyses. M.B., C.V., H.G., and R.I.M. wrote the manuscript. D.G., M.V., H.G., and R.I.M. designed and/or advised research. M.V., H.G., and R.I.M. should be considered joint senior authors.

ACKNOWLEDGMENTS

The authors thank the members of the R.I.M. laboratory, the Center for Cancer Systems Biology (CCSB), and Proteostasis Therapeutics for their support and critical reading of the manuscript. These studies were supported by Proteostasis Therapeutics, grants from the National Institutes of Health (NIGMS, NIA, and NIMH to R.I.M. and NHGRI P50HG004233 to M.V.), the Ellison Medical Foundation, a foundation that requests to be anonymous, and the Daniel F. and Ada L. Rice Foundation to R.I.M. M.V. is a "Chercheur Qualifié Honoraire" from the Fonds de la Recherche Scientifique (Wallonia-Brussels Federation, Belgium).

Received: May 20, 2014
Revised: September 5, 2014
Accepted: September 23, 2014
Published: October 23, 2014

REFERENCES

Ahn, Y.Y., Bagrow, J.P., and Lehmann, S. (2010). Link communities reveal multiscale complexity in networks. Nature *466*, 761–764.

Albanèse, V., Yam, A.Y., Baughman, J., Parnot, C., and Frydman, J. (2006). Systems analyses reveal two chaperone networks with distinct functions in eukaryotic cells. Cell *124*, 75–88.

Almeida, A., Bolaños, J.P., and Moreno, S. (2005). Cdh1/Hct1-APC is essential for the survival of postmitotic neurons. J. Neurosci. *25*, 8115–8121.

Balch, W.E., Morimoto, R.I., Dillin, A., and Kelly, J.W. (2008). Adapting proteostasis for disease intervention. Science *319*, 916–919.

Behrends, C., Langer, C.A., Boteva, R., Böttcher, U.M., Stemp, M.J., Schaffar, G., Rao, B.V., Giese, A., Kretzschmar, H., Siegers, K., and Hartl, F.U. (2006). Chaperonin TRiC promotes the assembly of polyQ expansion proteins into nontoxic oligomers. Mol. Cell *23*, 887–897.

Belin, A.C., and Westerlund, M. (2008). Parkinson's disease: a genetic perspective. FEBS J. *275*, 1377–1383.

Ben-Zvi, A., Miller, E.A., and Morimoto, R.I. (2009). Collapse of proteostasis represents an early molecular event in Caenorhabditis elegans aging. Proc. Natl. Acad. Sci. USA *106*, 14914–14919.

Berchtold, N.C., Cribbs, D.H., Coleman, P.D., Rogers, J., Head, E., Kim, R., Beach, T., Miller, C., Troncoso, J., Trojanowski, J.Q., et al. (2008). Gene expression changes in the course of normal brain aging are sexually dimorphic. Proc. Natl. Acad. Sci. USA *105*, 15605–15610.

Bocharova, N.A., Sokolov, S.S., Knorre, D.A., Skulachev, V.P., and Severin, F.F. (2008). Unexpected link between anaphase promoting complex and the toxicity of expanded polyglutamines expressed in yeast. Cell Cycle *7*, 3943–3946.

Brenner, S. (1974). The genetics of Caenorhabditis elegans. Genetics *77*, 71–94.

Cohen, E., Bieschke, J., Perciavalle, R.M., Kelly, J.W., and Dillin, A. (2006). Opposing activities protect against age-onset proteotoxicity. Science *313*, 1604–1610.

Cummings, C.J., Mancini, M.A., Antalffy, B., DeFranco, D.B., Orr, H.T., and Zoghbi, H.Y. (1998). Chaperone suppression of aggregation and altered subcellular proteasome localization imply protein misfolding in SCA1. Nat. Genet. *19*, 148–154.

Douglas, P.M., and Dillin, A. (2010). Protein homeostasis and aging in neurodegeneration. J. Cell Biol. *190*, 719–729.

Ehrnhoefer, D.E., Wong, B.K.Y., and Hayden, M.R. (2011). Convergent pathogenic pathways in Alzheimer's and Huntington's diseases: shared targets for drug development. Nat. Rev. Drug Discov. *10*, 853–867.

Gavin, A.C., Aloy, P., Grandi, P., Krause, R., Boesche, M., Marzioch, M., Rau, C., Jensen, L.J., Bastuck, S., Dümpelfeld, B., et al. (2006). Proteome survey reveals modularity of the yeast cell machinery. Nature *440*, 631–636.

Gidalevitz, T., Ben-Zvi, A., Ho, K.H., Brignull, H.R., and Morimoto, R.I. (2006). Progressive disruption of cellular protein folding in models of polyglutamine diseases. Science *311*, 1471–1474.

Gieffers, C., Peters, B.H., Kramer, E.R., Dotti, C.G., and Peters, J.M. (1999). Expression of the CDH1-associated form of the anaphase-promoting complex in postmitotic neurons. Proc. Natl. Acad. Sci. USA *96*, 11317–11322.

Haass, C., and Selkoe, D.J. (2007). Soluble protein oligomers in neurodegeneration: lessons from the Alzheimer's amyloid beta-peptide. Nat. Rev. Mol. Cell Biol. *8*, 101–112.

Hampel, H., Frank, R., Broich, K., Teipel, S.J., Katz, R.G., Hardy, J., Herholz, K., Bokde, A.L., Jessen, F., Hoessler, Y.C., et al. (2010). Biomarkers for

Alzheimer's disease: academic, industry and regulatory perspectives. Nat. Rev. Drug Discov. *9*, 560–574.

Harris, T.W., Antoshechkin, I., Bieri, T., Blasiar, D., Chan, J., Chen, W.J., De La Cruz, N., Davis, P., Duesbury, M., Fang, R., et al. (2010). WormBase: a comprehensive resource for nematode research. Nucleic Acids Res. *38*, D463–D467.

Hartl, F.U., and Hayer-Hartl, M. (2002). Molecular chaperones in the cytosol: from nascent chain to folded protein. Science *295*, 1852–1858.

Hartl, F.U., Bracher, A., and Hayer-Hartl, M. (2011). Molecular chaperones in protein folding and proteostasis. Nature *475*, 324–332.

Haslbeck, V., Eckl, J.M., Kaiser, C.J., Papsdorf, K., Hessling, M., and Richter, K. (2013). Chaperone-interacting TPR proteins in Caenorhabditis elegans. J. Mol. Biol. *425*, 2922–2939.

Hodges, A., Strand, A.D., Aragaki, A.K., Kuhn, A., Sengstag, T., Hughes, G., Elliston, L.A., Hartog, C., Goldstein, D.R., Thu, D., et al. (2006). Regional and cellular gene expression changes in human Huntington's disease brain. Hum. Mol. Genet. *15*, 965–977.

Hunter, S., Jones, P., Mitchell, A., Apweiler, R., Attwood, T.K., Bateman, A., Bernard, T., Binns, D., Bork, P., Burge, S., et al. (2012). InterPro in 2011: new developments in the family and domain prediction database. Nucleic Acids Res. *40*, D306–D312.

Jana, N.R., Tanaka, M., Wang, Gh., and Nukina, N. (2000). Polyglutamine length-dependent interaction of Hsp40 and Hsp70 family chaperones with truncated N-terminal huntingtin: their role in suppression of aggregation and cellular toxicity. Hum. Mol. Genet. *9*, 2009–2018.

Kamath, R.S., and Ahringer, J. (2003). Genome-wide RNAi screening in Caenorhabditis elegans. Methods *30*, 313–321.

Kim, A.H., Puram, S.V., Bilimoria, P.M., Ikeuchi, Y., Keough, S., Wong, M., Rowitch, D., and Bonni, A. (2009). A centrosomal Cdc20-APC pathway controls dendrite morphogenesis in postmitotic neurons. Cell *136*, 322–336.

Kitamura, A., Kubota, H., Pack, C.G., Matsumoto, G., Hirayama, S., Takahashi, Y., Kimura, H., Kinjo, M., Morimoto, R.I., and Nagata, K. (2006). Cytosolic chaperonin prevents polyglutamine toxicity with altering the aggregation state. Nat. Cell Biol. *8*, 1163–1170.

Kleizen, B., and Braakman, I. (2004). Protein folding and quality control in the endoplasmic reticulum. Curr. Opin. Cell Biol. *16*, 343–349.

Kuczera, T., Stilling, R.M., Hsia, H.E., Bahari-Javan, S., Irniger, S., Nasmyth, K., Sananbenesi, F., and Fischer, A. (2011). The anaphase promoting complex is required for memory function in mice. Learn. Mem. *18*, 49–57.

Langbehn, D.R., Brinkman, R.R., Falush, D., Paulsen, J.S., and Hayden, M.R.; International Huntington's Disease Collaborative Group (2004). A new model for prediction of the age of onset and penetrance for Huntington's disease based on CAG length. Clin. Genet. *65*, 267–277.

Li, M., Shin, Y.H., Hou, L., Huang, X., Wei, Z., Klann, E., and Zhang, P. (2008). The adaptor protein of the anaphase promoting complex Cdh1 is essential in maintaining replicative lifespan and in learning and memory. Nat. Cell Biol. *10*, 1083–1089.

Liang, W.S., Reiman, E.M., Valla, J., Dunckley, T., Beach, T.G., Grover, A., Niedzielko, T.L., Schneider, L.E., Mastroeni, D., Caselli, R., et al. (2008). Alzheimer's disease is associated with reduced expression of energy metabolism genes in posterior cingulate neurons. Proc. Natl. Acad. Sci. USA *105*, 4441–4446.

Link, C.D. (1995). Expression of human beta-amyloid peptide in transgenic Caenorhabditis elegans. Proc. Natl. Acad. Sci. USA *92*, 9368–9372.

Loerch, P.M., Lu, T., Dakin, K.A., Vann, J.M., Isaacs, A., Geula, C., Wang, J., Pan, Y., Gabuzda, D.H., Li, C., et al. (2008). Evolution of the aging brain transcriptome and synaptic regulation. PLoS ONE *3*, e3329.

López-Otín, C., Blasco, M.A., Partridge, L., Serrano, M., and Kroemer, G. (2013). The hallmarks of aging. Cell *153*, 1194–1217.

Maestre, C., Delgado-Esteban, M., Gomez-Sanchez, J.C., Bolaños, J.P., and Almeida, A. (2008). Cdk5 phosphorylates Cdh1 and modulates cyclin B1 stability in excitotoxicity. EMBO J. *27*, 2736–2745.

Marrocco, K., Thomann, A., Parmentier, Y., Genschik, P., and Criqui, M.C. (2009). The APC/C E3 ligase remains active in most post-mitotic Arabidopsis cells and is required for proper vasculature development and organization. Development *136*, 1475–1485.

Mayer, M.P. (2013). Hsp70 chaperone dynamics and molecular mechanism. Trends Biochem. Sci. *38*, 507–514.

Moran, L.B., Duke, D.C., Deprez, M., Dexter, D.T., Pearce, R.K., and Graeber, M.B. (2006). Whole genome expression profiling of the medial and lateral substantia nigra in Parkinson's disease. Neurogenetics *7*, 1–11.

Morley, J.F., Brignull, H.R., Weyers, J.J., and Morimoto, R.I. (2002). The threshold for polyglutamine-expansion protein aggregation and cellular toxicity is dynamic and influenced by aging in Caenorhabditis elegans. Proc. Natl. Acad. Sci. USA *99*, 10417–10422.

Nagaraj, N., Wisniewski, J.R., Geiger, T., Cox, J., Kircher, M., Kelso, J., Pääbo, S., and Mann, M. (2011). Deep proteome and transcriptome mapping of a human cancer cell line. Mol. Syst. Biol. *7*, 548.

Nollen, E.A., Garcia, S.M., van Haaften, G., Kim, S., Chavez, A., Morimoto, R.I., and Plasterk, R.H. (2004). Genome-wide RNA interference screen identifies previously undescribed regulators of polyglutamine aggregation. Proc. Natl. Acad. Sci. USA *101*, 6403–6408.

Park, S.H., Kukushkin, Y., Gupta, R., Chen, T., Konagai, A., Hipp, M.S., Hayer-Hartl, M., and Hartl, F.U. (2013). PolyQ proteins interfere with nuclear degradation of cytosolic proteins by sequestering the Sis1p chaperone. Cell *154*, 134–145.

Pearl, L.H., and Prodromou, C. (2006). Structure and mechanism of the Hsp90 molecular chaperone machinery. Annu. Rev. Biochem. *75*, 271–294.

Powers, E.T., and Balch, W.E. (2013). Diversity in the origins of proteostasis networks - a driver for protein function in evolution. Nat. Rev. Mol. Cell Biol. *14*, 237–248.

Powers, E.T., Morimoto, R.I., Dillin, A., Kelly, J.W., and Balch, W.E. (2009). Biological and chemical approaches to diseases of proteostasis deficiency. Annu. Rev. Biochem. *78*, 959–991.

Prodromou, C., Siligardi, G., O'Brien, R., Woolfson, D.N., Regan, L., Panaretou, B., Ladbury, J.E., Piper, P.W., and Pearl, L.H. (1999). Regulation of Hsp90 ATPase activity by tetratricopeptide repeat (TPR)-domain co-chaperones. EMBO J. *18*, 754–762.

Queitsch, C., Sangster, T.A., and Lindquist, S. (2002). Hsp90 as a capacitor of phenotypic variation. Nature *417*, 618–624.

Rutherford, S.L., and Lindquist, S. (1998). Hsp90 as a capacitor for morphological evolution. Nature *396*, 336–342.

Satyal, S.H., Schmidt, E., Kitagawa, K., Sondheimer, N., Lindquist, S., Kramer, J.M., and Morimoto, R.I. (2000). Polyglutamine aggregates alter protein folding homeostasis in Caenorhabditis elegans. Proc. Natl. Acad. Sci. USA *97*, 5750–5755.

Sayers, E.W., Barrett, T., Benson, D.A., Bolton, E., Bryant, S.H., Canese, K., Chetvernin, V., Church, D.M., Dicuccio, M., Federhen, S., et al. (2012). Database resources of the National Center for Biotechnology Information. Nucleic Acids Res. *40*, D13–D25.

Schmidt, M., and Finley, D. (2014). Regulation of proteasome activity in health and disease. Biochim. Biophys. Acta *1843*, 13–25.

Silva, M.C., Fox, S., Beam, M., Thakkar, H., Amaral, M.D., and Morimoto, R.I. (2011). A genetic screening strategy identifies novel regulators of the proteostasis network. PLoS Genet. *7*, e1002438.

Smoot, M.E., Ono, K., Ruscheinski, J., Wang, P.L., and Ideker, T. (2011). Cytoscape 2.8: new features for data integration and network visualization. Bioinformatics *27*, 431–432.

Song, Y., and Masison, D.C. (2005). Independent regulation of Hsp70 and Hsp90 chaperones by Hsp70/Hsp90-organizing protein Sti1 (Hop1). J. Biol. Chem. *280*, 34178–34185.

Tam, S., Geller, R., Spiess, C., and Frydman, J. (2006). The chaperonin TRiC controls polyglutamine aggregation and toxicity through subunit-specific interactions. Nat. Cell Biol. *8*, 1155–1162.

Tatsuta, T., Model, K., and Langer, T. (2005). Formation of membrane-bound ring complexes by prohibitins in mitochondria. Mol. Biol. Cell *16*, 248–259.

van Oosten-Hawle, P., Porter, R.S., and Morimoto, R.I. (2013). Regulation of organismal proteostasis by transcellular chaperone signaling. Cell *153*, 1366–1378.

Xu, J., Reumers, J., Couceiro, J.R., De Smet, F., Gallardo, R., Rudyak, S., Cornelis, A., Rozenski, J., Zwolinska, A., Marine, J.C., et al. (2011). Gain of function of mutant p53 by coaggregation with multiple tumor suppressors. Nat. Chem. Biol. *7*, 285–295.

Yu, A., Shibata, Y., Shah, B., Calamini, B., Lo, D.C., and Morimoto, R.I. (2014). Protein aggregation can inhibit clathrin-mediated endocytosis by chaperone competition. Proc. Natl. Acad. Sci. USA *111*, E1481–E1490.

Figure S1

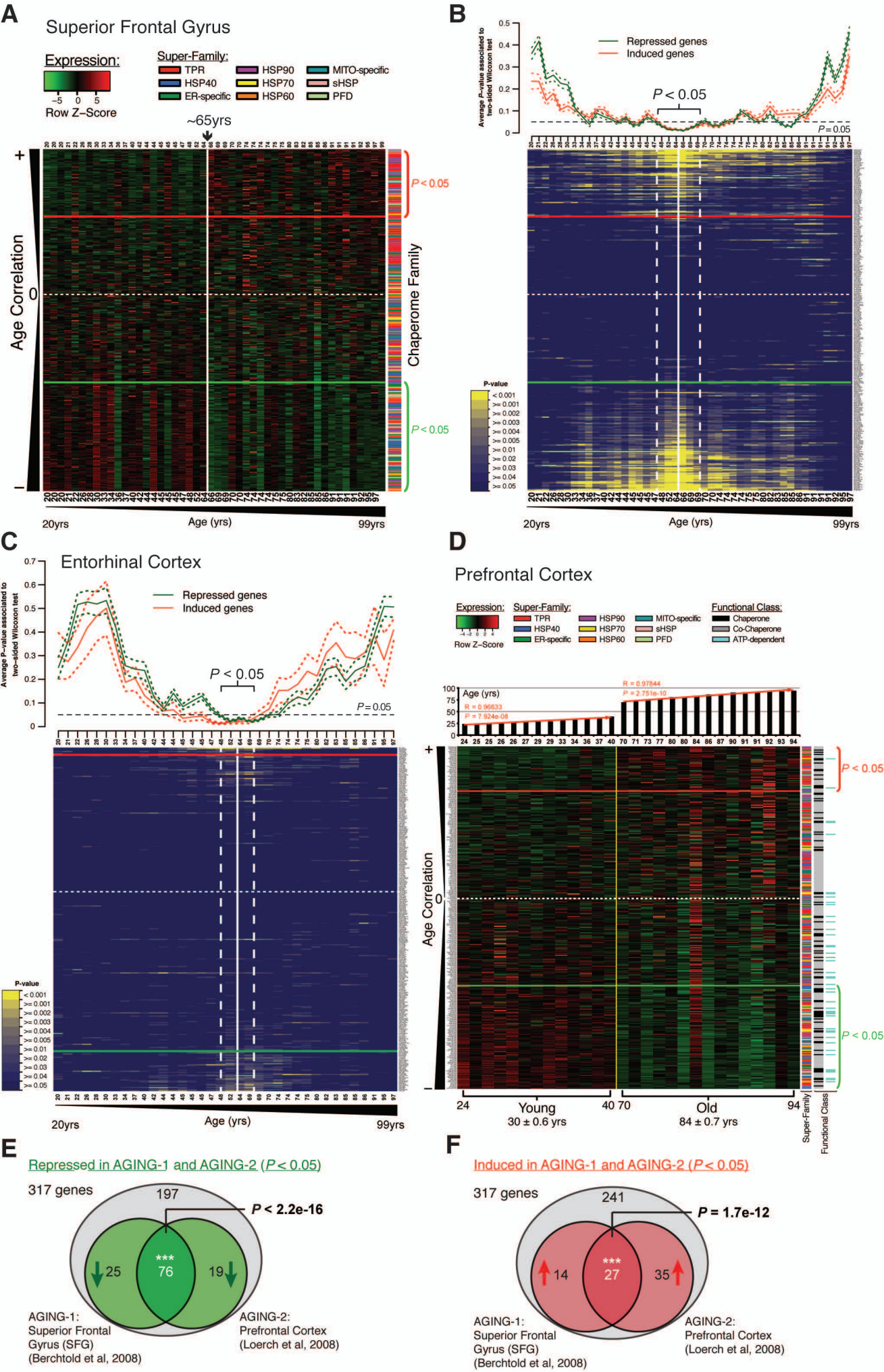
A
Superior Frontal Gyrus
Expression:
−5 0 5
Row Z–Score
Super-Family:
TPR
HSP40
ER-specific
HSP90
HSP70
HSP60
MITO-specific
sHSP
PFD
~65yrs
P < 0.05
Chaperome Family
P < 0.05
Age Correlation
+
0
–
20yrs
Age (yrs)
99yrs
B
Average P-value associated to two-sided Wilcoxon test
Repressed genes
Induced genes
P < 0.05
P = 0.05
P-value
< 0.001
>= 0.001
>= 0.002
>= 0.003
>= 0.004
>= 0.005
>= 0.01
>= 0.02
>= 0.03
>= 0.04
>= 0.05
20yrs
Age (yrs)
99yrs
C
Entorhinal Cortex
Average P-value associated to two-sided Wilcoxon test
Repressed genes
Induced genes
P < 0.05
P = 0.05
P-value
< 0.001
>= 0.001
>= 0.002
>= 0.003
>= 0.004
>= 0.005
>= 0.01
>= 0.02
>= 0.03
>= 0.04
>= 0.05
20yrs
Age (yrs)
99yrs
D
Prefrontal Cortex
Expression:
Row Z–Score
Super-Family:
TPR
HSP40
ER-specific
HSP90
HSP70
HSP60
MITO-specific
sHSP
PFD
Functional Class:
Chaperone
Co-Chaperone
ATP-dependent
Age (yrs)
R = 0.96633
P = 7.924e-08
R = 0.97844
P = 2.751e-10
P < 0.05
Age Correlation
+
0
–
P < 0.05
24
Young
30 ± 0.6 yrs
40 70
Old
84 ± 0.7 yrs
94
Super-Family
Functional Class
E
Repressed in AGING-1 and AGING-2 (P < 0.05)
317 genes
197
P < 2.2e-16
25
***
76
19
AGING-1:
Superior Frontal
Gyrus (SFG)
(Berchtold et al, 2008)
AGING-2:
Prefrontal Cortex
(Loerch et al, 2008)
F
Induced in AGING-1 and AGING-2 (P < 0.05)
317 genes
241
P = 1.7e-12
14
***
27
35
AGING-1:
Superior Frontal
Gyrus (SFG)
(Berchtold et al, 2008)
AGING-2:
Prefrontal Cortex
(Loerch et al, 2008)

Figure S2

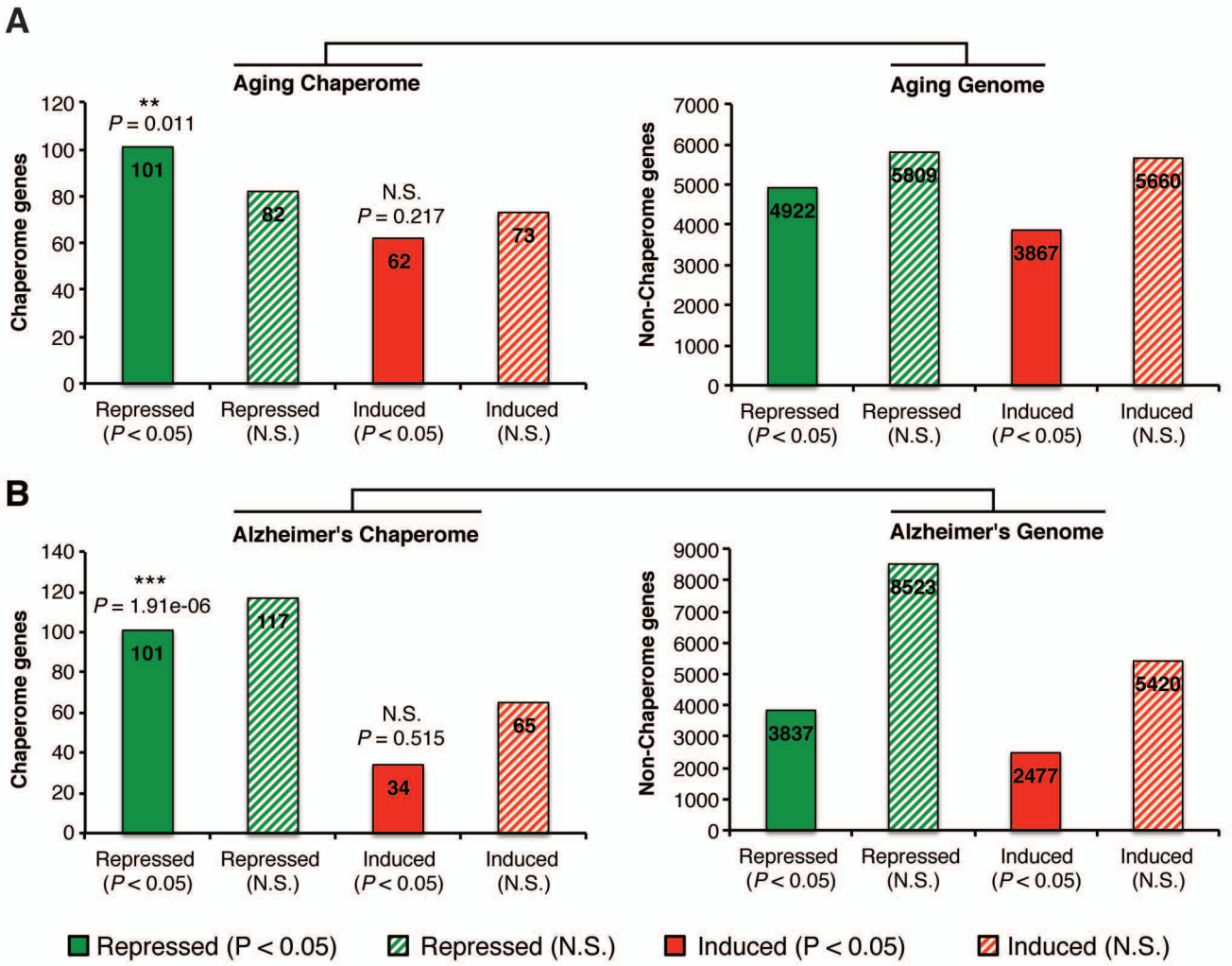
A
Aging Chaperome
Aging Genome
Chaperome genes
Non-Chaperome genes
** P = 0.011
N.S. P = 0.217
101
82
62
73
4922
5809
3867
5660
Repressed (P < 0.05)
Repressed (N.S.)
Induced (P < 0.05)
Induced (N.S.)
B
Alzheimer's Chaperome
Alzheimer's Genome
*** P = 1.91e-06
N.S. P = 0.515
101
117
34
65
3837
8523
2477
5420
Repressed (P < 0.05)
Repressed (N.S.)
Induced (P < 0.05)
Induced (N.S.)

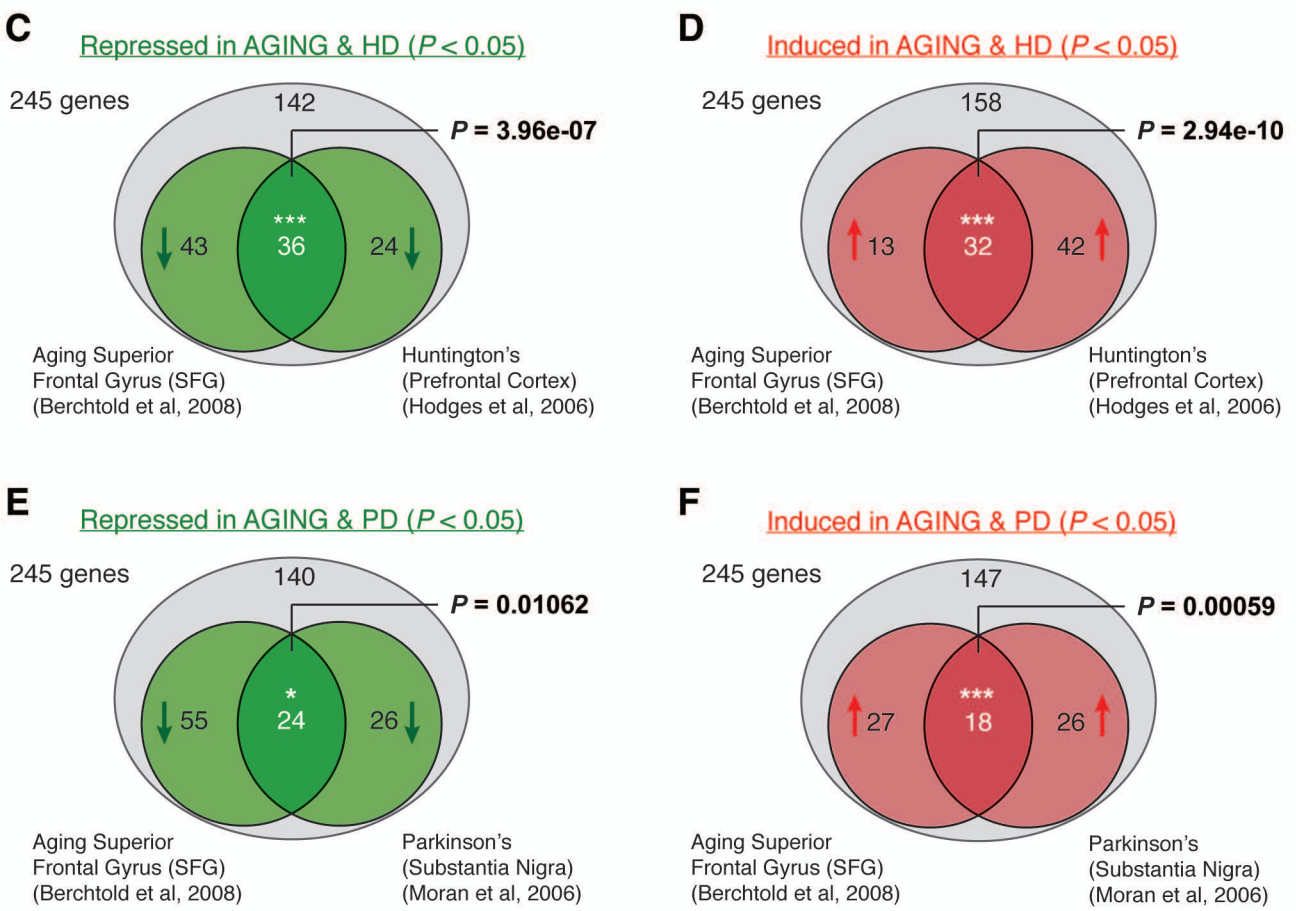
C
Repressed in AGING & HD (P < 0.05)
245 genes
142
P = 3.96e-07
43
***
36
24
Aging Superior Frontal Gyrus (SFG) (Berchtold et al, 2008)
Huntington's (Prefrontal Cortex) (Hodges et al, 2006)
D
Induced in AGING & HD (P < 0.05)
245 genes
158
P = 2.94e-10
13
***
32
42
Aging Superior Frontal Gyrus (SFG) (Berchtold et al, 2008)
Huntington's (Prefrontal Cortex) (Hodges et al, 2006)
E
Repressed in AGING & PD (P < 0.05)
245 genes
140
P = 0.01062
55
*
24
26
Aging Superior Frontal Gyrus (SFG) (Berchtold et al, 2008)
Parkinson's (Substantia Nigra) (Moran et al, 2006)
F
Induced in AGING & PD (P < 0.05)
245 genes
147
P = 0.00059
27
***
18
26
Aging Superior Frontal Gyrus (SFG) (Berchtold et al, 2008)
Parkinson's (Substantia Nigra) (Moran et al, 2006)

Figure S3

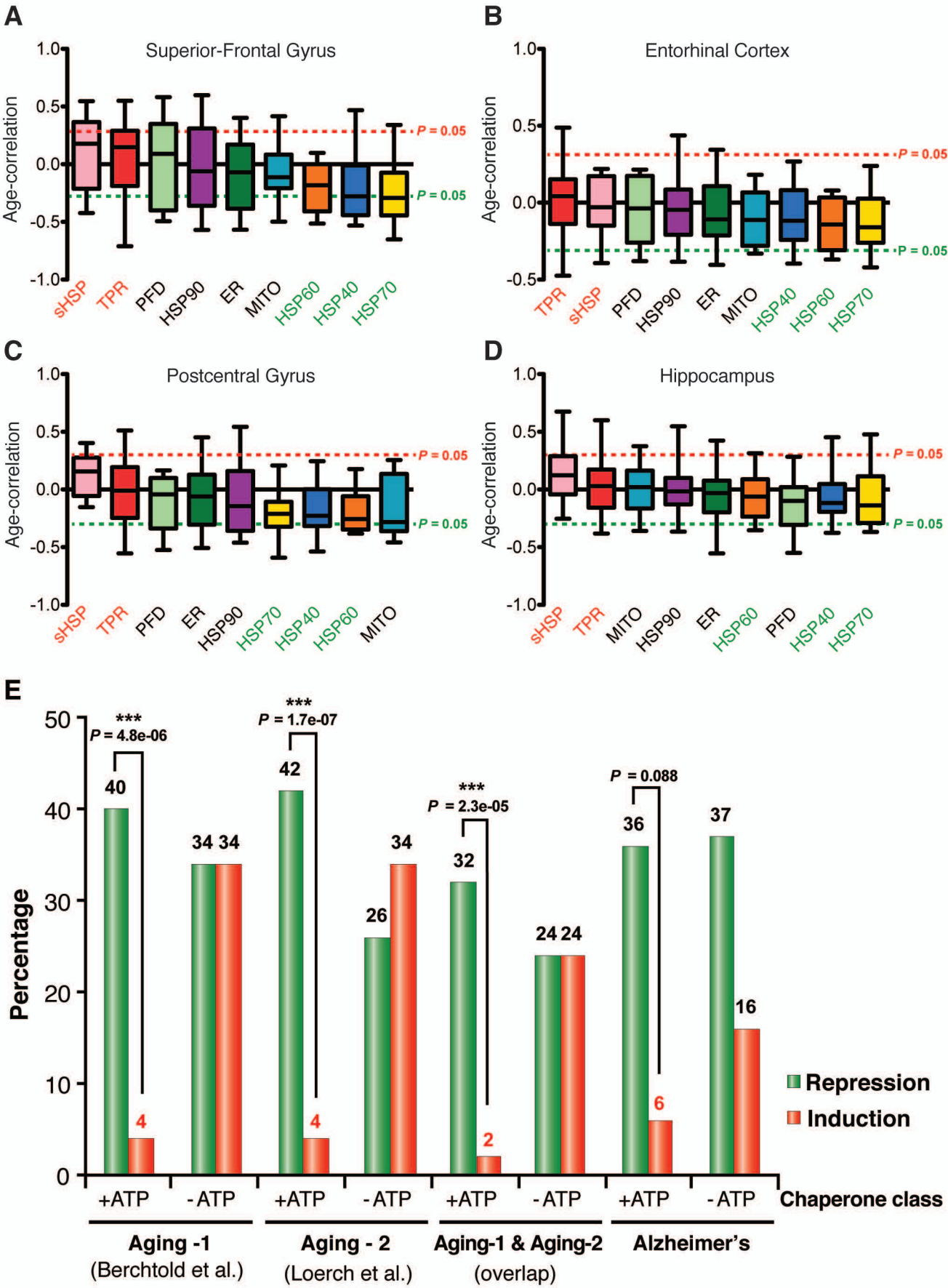
A
Superior-Frontal Gyrus
Age-correlation
1.0
0.5
0.0
-0.5
-1.0
P = 0.05
P = 0.05
sHSP
TPR
PFD
HSP90
ER
MITO
HSP60
HSP40
HSP70
B
Entorhinal Cortex
Age-correlation
P = 0.05
P = 0.05
TPR
sHSP
PFD
HSP90
ER
MITO
HSP40
HSP60
HSP70
C
Postcentral Gyrus
Age-correlation
P = 0.05
P = 0.05
sHSP
TPR
PFD
ER
HSP90
HSP70
HSP40
HSP60
MITO
D
Hippocampus
Age-correlation
P = 0.05
P = 0.05
sHSP
TPR
MITO
HSP90
ER
HSP60
PFD
HSP40
HSP70
E
Percentage
50
40
30
20
10
0
***
P = 4.8e-06
40
4
34 34
***
P = 1.7e-07
42
4
26
34
***
P = 2.3e-05
32
2
24 24
P = 0.088
36
6
37
16
Repression
Induction
+ATP
- ATP
+ATP
- ATP
+ATP
- ATP
+ATP
- ATP
Chaperone class
Aging -1
(Berchtold et al.)
Aging - 2
(Loerch et al.)
Aging-1 & Aging-2
(overlap)
Alzheimer's

Figure S4

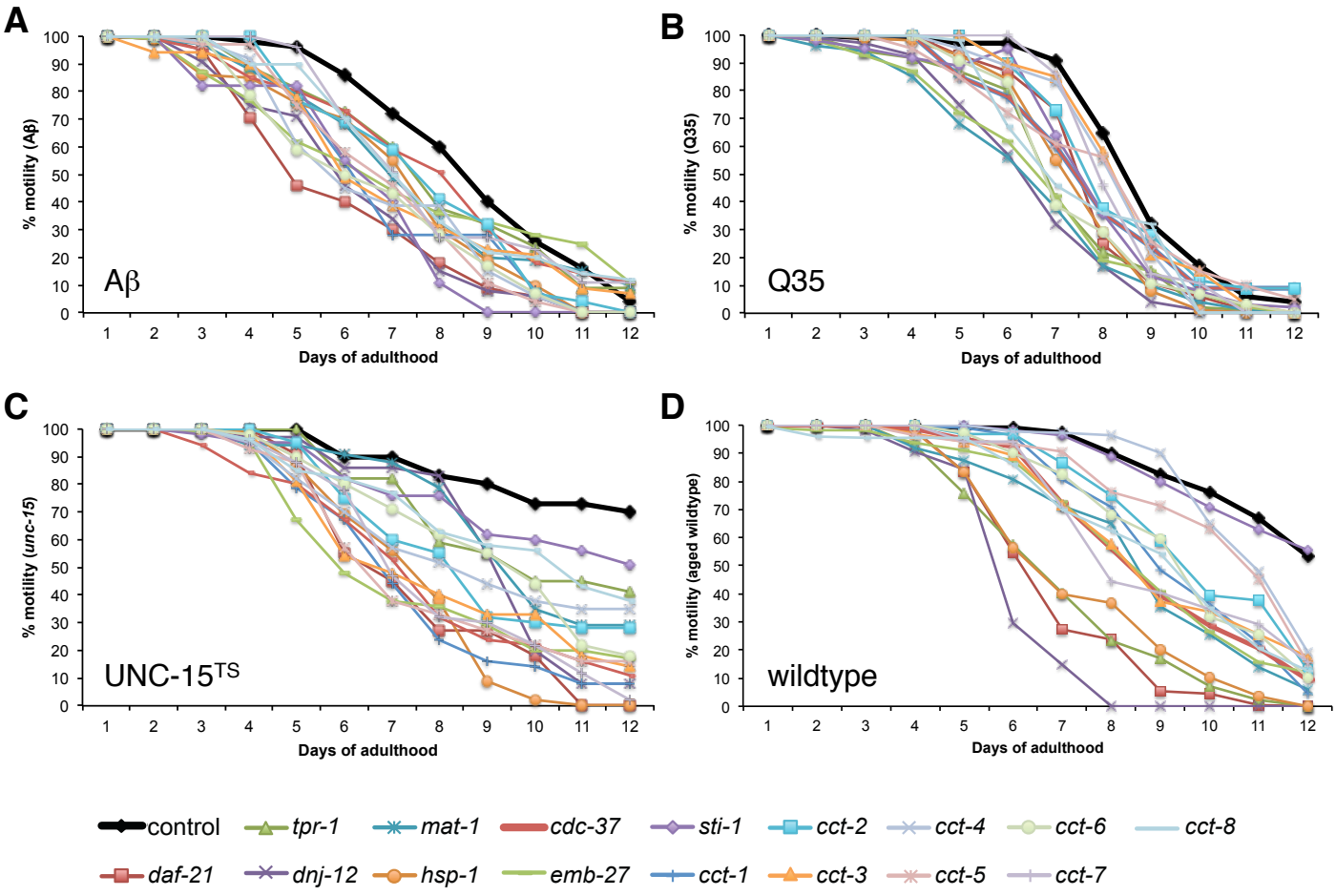
A
% motility (Aβ)
Aβ
Days of adulthood
B
% motility (Q35)
Q35
Days of adulthood
C
% motility (unc-15)
UNC-15TS
Days of adulthood
D
% motility (aged wildtype)
wildtype
Days of adulthood
control
tpr-1
mat-1
cdc-37
sti-1
cct-2
cct-4
cct-6
cct-8
daf-21
dnj-12
hsp-1
emb-27
cct-1
cct-3
cct-5
cct-7

Figure S5

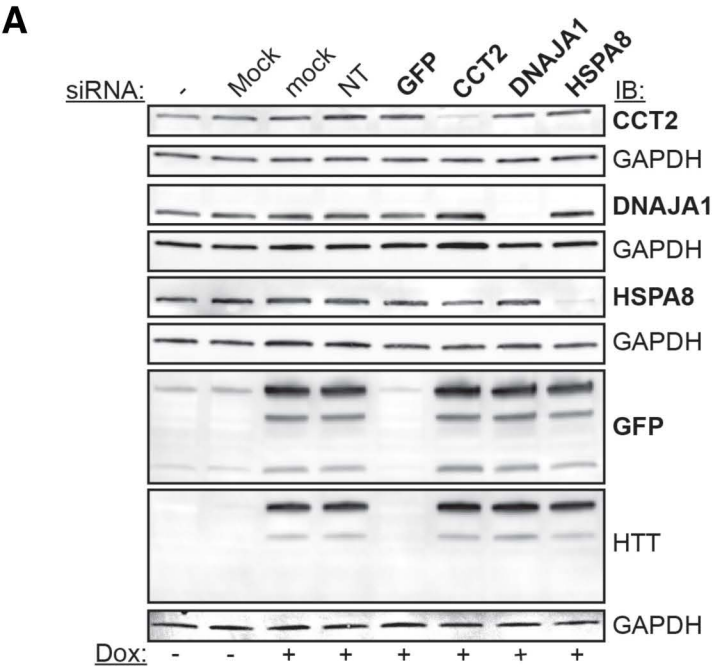

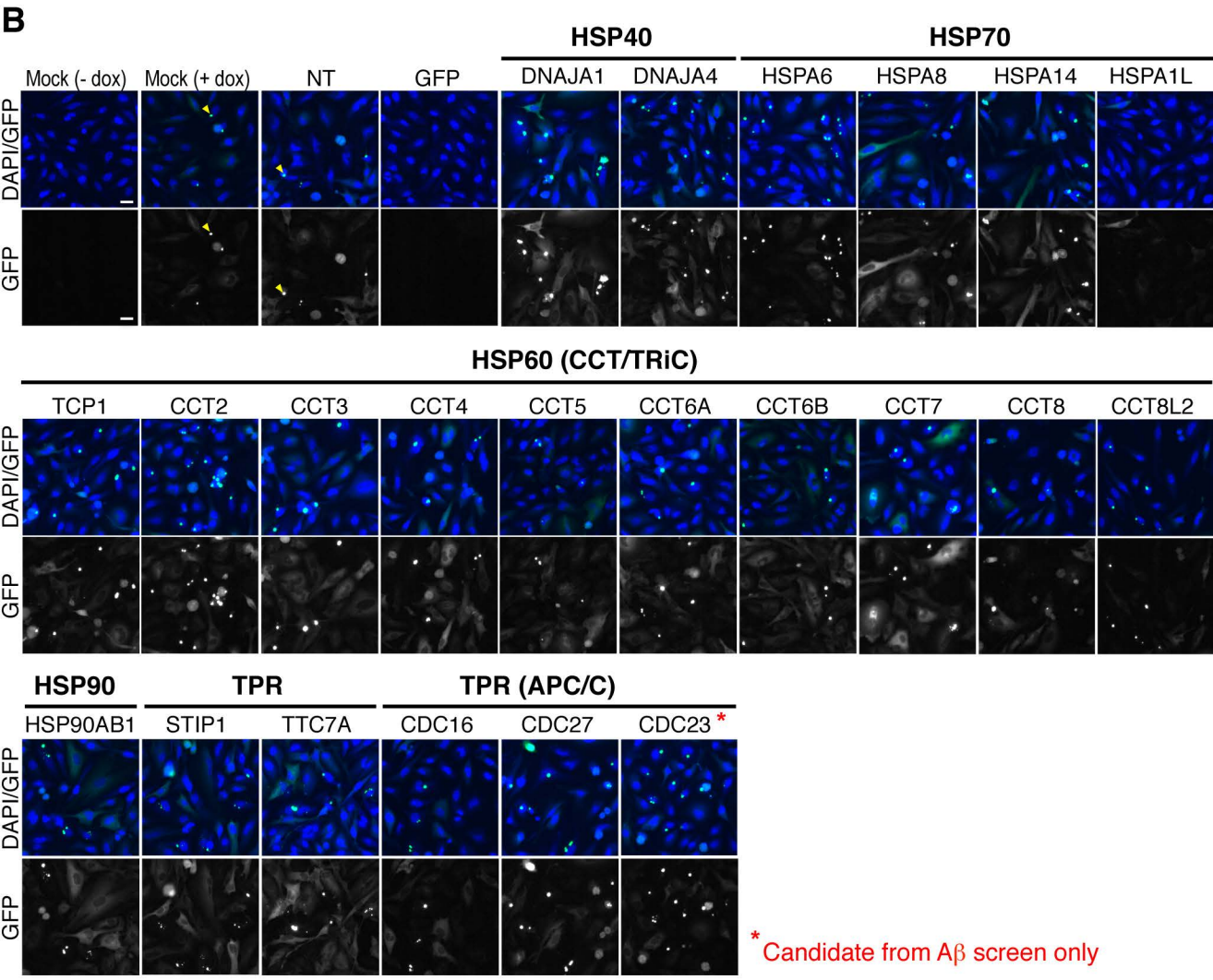

*Candidate from Aβ screen only

Figure S6

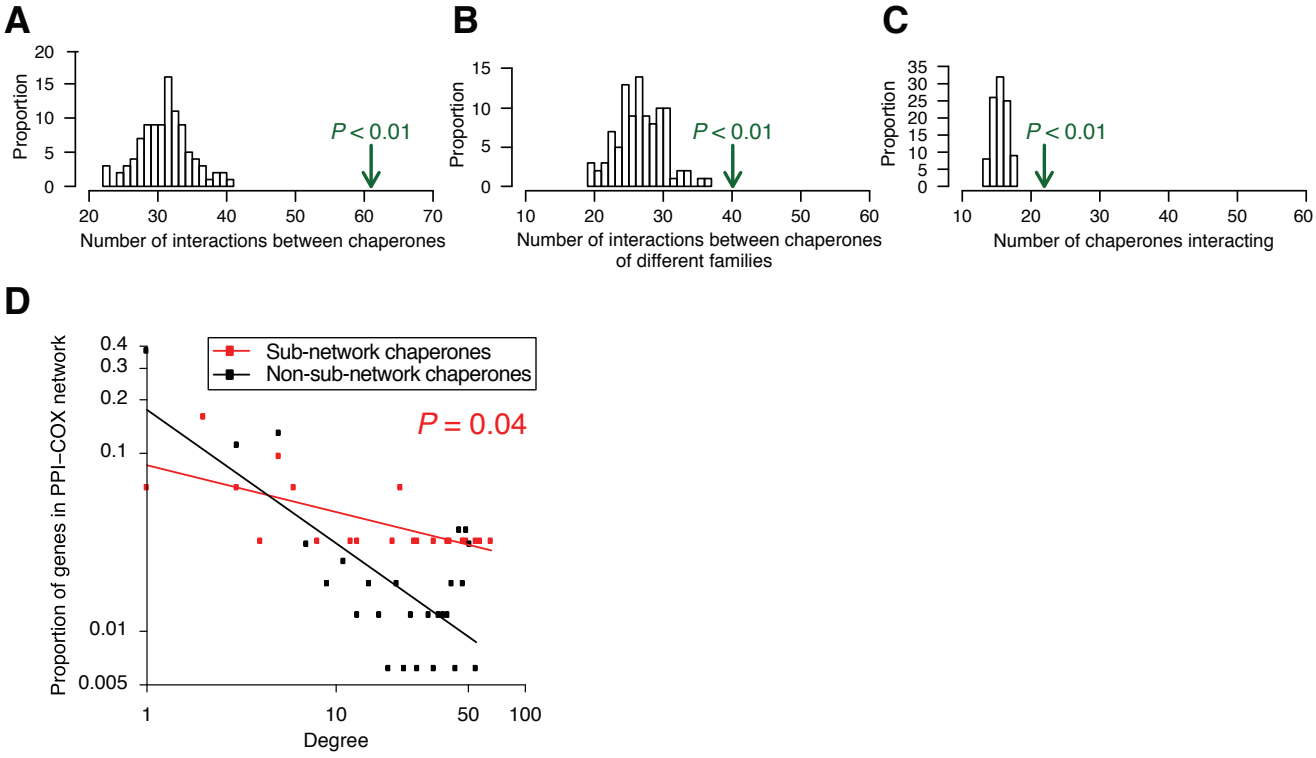
A
Proportion
P < 0.01
Number of interactions between chaperones
B
Proportion
P < 0.01
Number of interactions between chaperones of different families
C
Proportion
P < 0.01
Number of chaperones interacting
D
Sub-network chaperones
Non-sub-network chaperones
P = 0.04
Proportion of genes in PPI–COX network
Degree

Supplemental Figure Legends

Figure S1. Significant Clusters of Isochronic Differential Chaperome Induction and Repression in Human Aging Brains with Confirmation in an Independent Dataset, Related to Figure 1

A. Heat map showing 318 chaperones expressed in human brain (super frontal gyrus) ordered by decreasing correlation coefficients between age and gene expression (rows). Samples are ordered by chronologically increasing age with no clustering. The white dashed line indicates the gene with an age-expression correlation coefficient closest to zero. Chaperome genes above the red line are significantly induced by aging ($P < 0.05$), while the chaperone genes below the green line are significantly repressed by aging ($P < 0.05$). The y-axis color code visualizes the nine chaperome super-families. **B.** Two-sided Wilcoxon tests were performed on the chaperome aging heat maps to identify the age when the chaperome exhibits the most significant changes on the transcriptional level (Superior Frontal Gyrus). Genes are ordered by decreasing correlation of gene expression with age and samples are arranged by increasing age in chronological order to identify the age-span reflecting the most significant changes on the transcriptional level. Significant induction or repression of chaperones is observed between the early 50s to late 60s ($P < 0.05$) and peaks at ~65 years of age, which is also the mean age of onset of Alzheimer's Disease (Brookmeyer et al. 1998). **C.** Two-sided Wilcoxon tests performed as in B. on chaperome aging gene expression heat maps in Entorhinal Cortex. **D.** Heat map showing 318 chaperones expressed in human brain (Prefrontal Cortex) ordered by decreasing correlation coefficients between age and gene expression (rows). Samples are ordered chronologically by increasing age with no clustering (also see Figure S1). The white dashed line indicates the gene with an age-expression correlation coefficient closest to zero. Chaperome genes above the red line are significantly

induced by aging ($P < 0.05$), while the chaperone genes below the green line are significantly repressed by aging ($P < 0.05$). The y-axis color code visualizes from left to right the nine chaperome super-families, chaperone (black) and co-chaperone (grey) functional classes and ATP-dependent chaperones (turquoise) (compare Figure 1). **E-F.** Venn diagrams of genes significantly **E)** repressed ($P < 2.2e-16$) and **F**) induced ($P = 1.7e-12$) in comparable tissues from two independent datasets of human brain aging overlap significantly. Datasets used: AGING-1: Super Frontal Gyrus, aging dataset GSE11882 (Berchtold et al. 2008); AGING-2: Prefrontal Cortex, aging dataset (PMID:18830410) (Loerch et al. 2008).

Figure S2. Significance of Broad Chaperome Repression in Human Brain Aging and Alzheimer's Disease Compared to the Global Trend in the Genome and Significant Overlap of Chaperome Repression and Induction between Aging and Disease, Related to Figures 1 and 2

A. Broad repression of 32% (101 genes) of chaperome genes expressed in human aging brain (Superior Frontal Gyrus, (Berchtold et al. 2008)) is significant ($P = 0.01098$) compared to the global repression trend in the genome (20,258 genes, of which 4,922 non-chaperome genes are significantly repressed), while chaperome induction is not significant. **B.** Concordantly, broad repression of 32% (101 genes) of chaperome genes expressed in brains (Superior Frontal Gyrus, (Liang et al. 2008)) of Alzheimer's disease patients compared to age-matched controls is also significant (*** $P = 1.908e-06$) compared to the global trend in the genome (20,257 genes, of which 3,837 non-chaperome genes are significantly repressed), while induction of chaperome genes is not significant. **C-E.** Venn Diagrams showing overlaps between significantly induced and repressed human chaperome genes. Datasets used: AGING-1: Super Frontal Gyrus (SFG), dataset GSE11882 by Berchtold et al, PNAS 2008;

HD: Prefrontal Cortex (PFC), dataset GSE3790 (Hodges et al. 2006); PD: Substantia Nigra (SN), dataset GSE20295 (Moran et al. 2006). Chaperones and co-chaperones significantly induced and repressed ($P < 0.05$) in aging human brains and brains from AD patients compared to controls were identified amongst 317 chaperones and co-chaperones expressed in human brain and detected in both corresponding datasets. **C-D.** Overlap between genes significantly repressed or induced in SFG of human aging brain and in PFC of HD patients are significant. **E-F.** Overlaps between genes significantly repressed or induced in SFG of human aging brain and in SN of PD patients are significant.

Figure S3. Reproducible Functional Family Distribution of Chaperome Gene Expression Dynamics in Four Different Tissues from Human Aging Brains and Preferential Repression of ATP-dependent over ATP-independent Chaperones, Related to Figures 1 and 2

A-D. Boxes and Whiskers plots showing range of aging-correlation of each chaperome functional family and overall family distribution of aging-correlation arranged by decreasing median age-correlation for each super-family. Whiskers indicate minimum and maximum age-correlation observed amongst members of each super-family. Boxes outline the 25^{th} and 75^{th} percentile. Bars indicate the median age-correlation amongst all members of the super-family. Age-correlation observed for repressed and induced genes at *P*-value cut-off $P = 0.05$ in each dataset is indicated. Tissues are: **A:** Superior Frontal Gyrus, **B:** Entorhinal Cortex**, C:** Postcentral Gyrus**,** and **D:** Hippocampus. Dataset GSE11882, (Berchtold et al. 2008). **E.** Comparison of % fractions of ATP-dependent (total = 50) and ATP-independent (total = 38) chaperones present in the respective sets of significantly induced or significantly repressed genes in 1) Aging Super Frontal Gyrus (SFG), Aging-1 dataset GSE11882, (Berchtold et al.

2008); 2) Aging Prefrontal Cortex, Aging-2 dataset (PMID:18830410), (Loerch et al. 2008); 3) Superior Frontal Gyrus of Alzheimer's Disease patients versus controls (AD) gene expression dataset (GSE5281),(Liang et al. 2008).

Figure S4. Chaperome Subset RNAi significantly enhances paralysis phenotypes, Related to Figures 3 and 4

Individual data points shown for chaperome subset RNAi functional data shown in Figure 3 G and H and Figure 4 A and B. **A.** RNAi paralysis phenotype (% motility) observed in $A\beta_{42}$ expressing *C. elegans* throughout adulthood (days 1 to 12). Data points are means (n ≥ 3 independent experiments and n ≥ 25 animals / trial). **B.** RNAi paralysis phenotype (% motility) observed in Q35 expressing *C. elegans* throughout adulthood. Data points are means (n ≥ 3 independent experiments and n ≥ 25 animals / trial). **C.** RNAi paralysis phenotype (% motility) observed in *unc-15(e1402)* TS-strain at 15ºC throughout adulthood. Data points are means (n ≥ 3 independent experiments and n ≥ 20 animals / trial). **D.** RNAi paralysis phenotype (% motility) observed in aged wild-type-animals throughout adulthood. Data points are means (n ≥ 3 independent experiments and n ≥ 20 animals / trial).

Figure S5. The Human Chaperome Subset Safeguards Proteostasis to Prevent Huntingtin Aggregation, Related to Figure 5

A. Validation of siRNA knockdown efficiency of HTT-GFP, CCT2, DNAJA1 and HSPA8 by immunoblotting. **B.** Representative cellular images for siRNA knock-down of GFP (positive control) and chaperome sub-netowork targets representative of the five functional chaperome families present in the chaperome subset (HSP40s, HSP60s, HSP70s, HSP90s, TPR (APC/C)) are shown. NT = non-targeting siRNA. The yellow arrows highlight Htt-GFP aggregates. Scale bar, 20μm.

Figure S6. Significance of Human Chaperome Sub-Network Network Inter-Connectivity, Related to Figure 6

A-C. Significant inter-connectivity of the human orthologous chaperome sub-network interactome compared to 100 randomized PPI-COX chaperome networks. PPI-COX network randomizations were performed keeping the number of nodes, edges and node degree constant while rewiring edges between nodes. PPI and COX edges were treated separately. **A.** Number of interactions between chaperones, **B.** number of interactions between chaperones of different families, and **C.** the number of chaperones interacting were significant ($P < 0.01$) compared to the numbers observed in 100 randomized PPI-COX networks. **D.** Proportion of genes in the PPI-COX network and their degree distribution. Sub-network chaperones have a significantly higher degree than the rest of the PPI-COX chaperome network nodes, i.e. non-sub-network chaperones ($P = 0.04$, Wilcoxon test).

Supplemental Table Legends

Table S1. Chaperome Super-Family InterPro Criteria Domains, Related to Figure 1

44 unique IPR-IDs representing *bona-fide* InterPro domains used as criteria domains for chaperome gene list curation and annotation into 9 functional super-families. IPR-IDs, corresponding *bona-fide* functional chaperone and co-chaperone families, respective parent super-families as well as super-family color-codes are indicated.

Table S2. The Chaperome Database, Related to Figures 1 and 3

Tab S2A. 332 human chaperones and co-chaperones constituting the human chaperome. Uniprot identifier, HGNC gene symbol, InterPro domains and match to our chaperome

ontology categorization, chaperome family ontology, compartment, gene name, gene description as well as worm orthologs are indicated. Related to Figure 1. **Tab S2B.** 219 worm chaperones and co-chaperones constituting the worm chaperome. ENSEMBL identifier, WBase gene ID and gene symbol, InterPro domains and match to our chaperome ontology categorization, chaperome family ontology, compartment, gene name, gene description as well as human orthologs are indicated. Related to Figure 3.

Table S3. Human Chaperome Gene Expression Correlation in Brain Aging and Disease, Related to Figures 1 and 2

Tab S3A. 318 human chaperome genes ordered by their correlation of gene expression with age in Superior Frontal Gyrus, Postcentral Gyrus, Entorhinal Cortex and Hippocampus of human brains (Berchtold et al. 2008) in decreasing order. * $P < 0.05$, ** $P < 0.01$, *** $P < 0.001$, Student's t test. **Tab S3B.** 318 human chaperome genes ordered by their correlation of gene expression with age in Prefrontal Cortex of human brain (Loerch et al. 2008) in decreasing order. * $P < 0.05$, ** $P < 0.01$, *** $P < 0.001$, Student's t test. **Tab S3C.** 318 human chaperome genes ordered by their correlation with gene expression in human brain Superior Frontal Gyrus (Berchtold et. al, PNAS 2008) in decreasing order. Correlation of gene expression in the three neurodegenerative diseases AD ((Liang et al. 2008)), HD (Hodges et al. 2006) and PD (Moran et al. 2006) is indicated as ratio over normal (control patients). **Tab S3D.** Overlaps of human chaperome genes significantly repressed in Aging (Superior Frontal Gyrus, (Berchtold et al. 2008)) and significantly repressed in AD (Superior Frontal Gyrus), HD (Prefrontal Cortex) and/or PD (substantia nigra). AD, HD, and PD disease gene expression datasets are from: AD (Liang et al. 2008), HD (Hodges et al. 2006) and PD

(Moran et al. 2006). **Tab S3E.** Overlaps of human chaperome genes significantly induced in Aging and significantly induced in AD, HD and/or PD. Tissues and datasets as in Tab S3A.

Table S4. Human Chaperome Physical Protein-Protein Interactions, Related to Figures 2 and 6

Tab S4A. 206 unique protein-protein interactions between human brain-expressed chaperones from public databases. Source database name, cited publication (PubMed ID) and interaction discovery method are indicated, respectively. **Tab S4B.** 40 homodimers were excluded from the network analysis.

Table S5. Human Chaperome Brain Aging Co-Expression Correlation, Related to Figures 2 and 6

50,403 all-by-all pairs representing 318 human chaperome genes expressed in human brain (Superior Frontal Gyrus, (Berchtold et al. 2008)). Pearson co-expression correlation coefficients for each pair were calculated based on gene expression in human brain. COX edges with a Pearson co-expression correlation coefficient with aging (corr > 0.8) were designated as COX. 1,193 COX edges represent significantly co-expressed chaperones in human brains.

Table S6. Human Chaperome Physical and Brain Co-Expression Chaperome Network and Aging-Response Communities, Related to Figures 2 and 6

Tab S6A. In this network, there are 5,004 pairs of interactions, of which 714 are PPIs, 4,226 are COX (corr > 0.8), and 64 are both PPI and COX. There are 66 pairs in induction communities and 4,098 pairs in repression communities. The unique pairs are in parentheses

and listed separately in **Tab S6B**. There is a total of 40 communities, of which 6 are induction communities and 34 are repression communities.

Table S7. Human Chaperome Sub-Network Functional Validation, Related to Figures 3, 4, and 5

16 C. elegans chaperone and co-chaperone hits from Ab and polyQ RNAi screens constituting the "chaperome subset". Paralysis phenotypes are indicated as % motility. 28 human orthologs are color-coded according to their siRNA phenotype in a HeLa cellular model of Huntingtin-exon1(Q78)-GFP cytoplasmic clearance and aggregation.

Supplemental Experimental Procedures

Chaperome Gene List Curation, Annotation and Orthology Mapping

We curated the literature for chaperone and co-chaperone families covering all structural and functional categories and the major subcellular localizations relevant to chaperone-assisted protein folding and annotated family members known at present for human and *C. elegans* in detail including for human the respective Entrez gene IDs, Uniprot identifiers, gene symbols, cellular compartment, Uniprot description and Entrez gene description (Chang et al. 2007; Tang et al. 2007; Heldens et al. 2010; Braakman and Bulleid 2011). We then matched domain structures as referenced by the UniProt database to each gene and prioritized *bona-fide* InterPro protein domain identifiers (IPR-IDs) characteristic of each family to i) consolidate our literature-based annotation and ii) to search for additional structurally similar family members not previously associated with the respective families in the literature. We determined 9 top-level functional chaperome super-families based on curated literature evidence as well as based on a curated selection of *bona-fide* IPR-domains (referenced by IPR-IDs) (Table S1)

found in these established functional families. Chaperones and co-chaperones curated in the literature as members of one of these nine super-families or genes containing at least one of these IPR-domains were consequently grouped accordingly into the nine functional super-families, including the HSP60, HSP70, HSP90 and Prefoldin (PFD) folding machines, small HSPs (sHSPs). The specific complement of chaperones that have evolved to function exclusively within the ER and mitochondrial (MITO) subcellular compartment were grouped as 'ER-specific' and 'MITO-specific'. Smaller co-chaperone families such as the cyclophilins, FKBPs with clear functional association with a chaperone host were concordantly co-grouped within the respective chaperone system, such as the HSP90 system or the HSP70 system in the case of Bag proteins or the GrpE nucleotide exchange factors (NEFs). More promiscuous co-chaperones such as the HSP40 and TPR-domain containing co-chaperones, however were grouped as separate super-families. Consequently chaperome super-family grouping was systematic such that we first considered a guilt-by-association principle for specific pre-curated sets of *bona-fide* IPR criteria domains. Consequently, chaperones were grouped by their functionality first, regardless of their subcellular localization. MITO-specific and ER-specific super-family members represent those chaperones and co-chaperones, for which no IPR-domain match strings were obtained. These were curated and grouped based on on literature knowledge and functional evidence of compartment-specific localization and/or function.

To complement human and worm chaperome gene set annotations with phylogenetic relationships between the two species we identified human and worm orthologues by automated orthology mapping using the NCBI HomoloGene database. In a second step we re-curated the annotations based on the WormBase database (release WS234) comparative genomics tool, which associates each worm gene entry with human orthologous based on

curated and automated predictions by NCBI KOGS, InParanoid, TreeFam, precomputed BLAST results, Ensembl COMPARA and the orthologs matrix project (OMA) (Harris et al. 2010; 2012; Sayers et al. 2012). We applied bipartite mapping according to our annotation criteria to compare worm and human chaperomes and identified the overlapping as well as the respective species-specific chaperome subsets.

Chaperome Expression Correlation Analyses

We extracted expression profiles for 318 human chaperome genes from human Superior Frontal Gyrus, Entorhinal Cortex, postcentral gyrus and Hippocampus brain biopsy tissue samples of aged subjects (dataset accessible under GEO accession number GSE11882) (Berchtold et al. 2008) and from an additional independent dataset derived from human Prefrontal Cortex (Loerch et al. 2008). Original expression data are fitted by linear model using R package Limma at log2 scale, with age and gender as variables. After model fitting, we subtracted the portion of gene expression associated with gender cofactor so that the processed data are only associated with age cofactor. Among multiple probe sets of a gene, we kept the probe set whose expression was most significantly changed with age, according to the adjusted *P*-value associated with the coefficient of age cofactor in the linear model. Chaperome age expression correlation coefficients (corr) and *P*-values were calculated using cor.test function in the R stats package and applying default arguments. Chaperome genes with significantly induced or repressed expression during human brain aging were identified at a *P*-value cutoff of < 0.05. We used distance measures defined by 1-[Pearson_correlation_coefficient] to create a distance matrix comparing chaperome pairs, where correlation coefficients were calculated using the cor function in the R stats package applying default arguments. Hierarchical clustering was performed on the calculated distance matrix using hclust in the R stats package with default arguments and displayed as a heat

map with dendrogram using heatmap.2 in the R gplots package and dendrogram display. To estimate chaperome induction and repression cluster boundaries we ordered aging samples chronologically from 20 to 99 years old. We computed Wilcoxon signed-rank tests (Bauer 1972) for each chaperome gene at each age to evaluate the difference between the expression values of the gene below and above that specific age (the corresponding age cutoff being categorized in the higher age category) and the significances were estimated by the *P*-value of the Wilcoxon test. We averaged *P*-value obtained for all genes at each age cutoff to determine overall most significant age. Brain biopsy samples from AD, PD and HD patients were analyzed as described above. Correlation of expression was determined as ratio of average expression in disease over controls.

Chaperome Network Community Clustering

Genes significantly induced or repressed in aging with $P < 0.05$ were defined as significantly aging-correlated. We analyzed the PPI-COX network to identify clusters of edges that connect subsets of nodes using the link-community algorithm (Ahn et al. 2010), which allows clustering of graph edges such that nodes can be part of different communities. We considered communities with ≥ 2 edges and thus ≥ 3 nodes, and containing only induced or only repressed nodes. Link communities are based on significance of aging-correlation and network connectivity taking both PPI and COX edges into account. Controlled by network randomization trials this approach allowed us to re-prioritize 15 genes not significantly aging-correlated ($P \geq 0.05$) based on their membership in link communities and to de-prioritize 35 genes with significant aging-correlation based on their absence from communities.

In order to evaluate connectivity of the chaperome network, we built 100 randomized PPI-COX networks, keeping the number of nodes, edges and node degrees constant while

rewiring edges between nodes. PPI and COX edges were treated separately to conform to the different nature of the interaction.

C. elegans RNAi Screens for Chaperome Modifiers of Protein Misfolding, Aging-related Proteotoxicity and Myofilament Structure

We performed chaperome-wide RNAi screens for enhancement of motility defects in *C. elegans* muscle cells with the commercial RNAi library and additional candidates cloned into L4440, transformed into *E. coli* strain HT115(DE3) (Kamath and Ahringer 2003). RNAi bacterial cultures were grown for 12 hours in LB-ampicillin 50 ug/ml, at 37°C and induced with 1mM isopropyl B-D-thiogalatoside (IPTG, Sigma) for 4 hours at 37°C. Cultures were plated on agar containing IPTG (1.429 g/L), ampicillin (.075 g/L), and tetracycline (.0125 g/L). To obtain an age-synchronized population, eggs were harvested from gravid hermaphrodites, hatched overnight at 20°C and arrested at the first larval stage (L1). The next day, 35-40 arrested L1 worms were plated on agar with chaperome RNAi bacteria and incubated at 20°C. Adult worms were transferred to new RNAi plates daily to separate adults from progeny, and scored for paralysis ($A\beta_{42}$ screen) on day 4 or for motility defects (Q35 screen) on day 2 of adulthood.

Aβ expressing worms that did not move when prodded with a needle were scored as paralyzed (Link 1995). Q35 expressing worms' movements were digitally recorded using a Leica M205 FA microscope with a Hamamatsu digital camera C10600-10B and the Hamamatsu SimplePCI imaging software. Animal positions were determined using ImageJ. Animals were tracked throughout a 30-second movie and track-length was calculated as sum of lengths of all movement vectors. Average speed (pixels per frame) was the sum of all movement vectors divided by the total number of vectors (tracks). Speeds were converted from pixels per frame into μm/s (Silva et al. 2011). RNAi modifiers causing larval delays or

arrest were retested and fed to animals at L4 larval stage. RNAi modifiers, such as *unc-45*, that affected the motility of wildtype animals to the same extent during our screens were removed from further analysis. Animals fed chaperome candidates RNAi with a 20% decrease in movement compared to control animals were retested and RNAi candidates with a 20% decrease in movement compared to control in ≥ 3 experiments constitute the final set. For aging-related proteotoxicity, synchronized L1 animals expressing $A\beta_{42}$, polyQ or wild-type animals were fed bacteria expressing RNAi for each subset chaperone. When lethality or larval arrest were observed worms were fed at the L4 stage. Adult animals were assayed daily and those that did not respond to gentle prodding were scored as paralyzed. *unc-15(e1402)* animals were grown at 15°C and assayed daily for paralysis.

To examine the effect of chaperome subset gene down-regulation on myofilament folding and assembly in muscle cells (Herndon et al. 2002) (Sarcopenia readout), we monitored MYO-3::GFP fluorescence in animals fed with bacteria expressing dsRNA against each subset chaperone. Images were taken on day 1 and day 8 of adulthood using a Zeiss Axiovert 200 microscope.

siRNA Perturbation Coupled to High-Content Imaging (siRNA-HCI) Screen for Modifiers of Huntingtin (HTT) Cytoplasmic Clearance and Aggregation in HeLa Cells

Chaperome modifiers of Htt cytoplasmic clearance and aggregation were identified by siRNA perturbation coupled to high-content imaging (siRNA-HCI) in HeLa cells. Monoclonal doxycycline-inducible Tet-On HeLa cells expressing HTT(Q78)-exon1-GFP from a P_{CMV} promoter in the pLenti6.3/V5 vector were maintained in Dulbecco's Modified Eagle's Medium (DMEM) with 10% FBS, 1% penicillin/streptomycin (P/S), 2µg/ml Blasticidin and 200µg/ml G418. siRNA knock-downs were performed in 96-wells at initial cell density of 8,000 cells/well in 100µl DMEM and 10% FBS and 1% P/S. Twelve hours post seeding, cells were

mock - treated or treated with 10nM non-targeting, GFP or target-specific quadruplex Dharmacon smart-pool siRNAs in Optimem and 0.5µl Dharmafect #1. Twelve hours post transfection media were replaced and Htt(Q78)-exon1-GFP expression induced with 0.5µg/ml dox for 48 hours. After 72 hours of siRNA knock-down and 48 hours of induction, cells were fixed in para-formaldehyde and nuclei stained with Hoechst 33342 dye. Fixed cells were imaged using a Thermo Scientific Cellomics ArrayScan VTI HCS Reader. Cell number and % cells with one or more aggregates were quantified using co-localization and compartmental analysis algorithms. Knock-downs were carried out in triplicate and two biological repeats. Percentage of cells with ≥ one aggregate per cell were determined over doxycycline-induced mock-treated cells.

Immunoblot Validation of Chaperome Sub-Network siRNA Knockdown

Monoclonal doxycycline-inducible Tet-On HeLa cells expressing HTT(Q78)-exon1-GFP were maintained in DMEM medium under Blasticidin and G418 selection. siRNA knock-downs were performed as described above in 6-wells at initial cell density of 250,000 cells/well. After 72 hours of siRNA knockdown and 48 hours of induction, cells were washed in 1x PBS and lysed in 1x RIPA buffer with Roche Complete Mini protease inhibitor cocktail. Protein extracts were prepared in RIPA buffer and 10µg extract were separated by SDS-PAGE, probed with primary antibodies and consequently HRP-coupled secondary antibodies followed by chemoluminescent detection. Primary antibodies used were anti-CCT2, Cell Signaling #3561 rabbit polyclonal IgG at 1:1000 dilution; anti-DNAJA1 (HDJ2), Abcam ab126774 [EPR7248] rabbit monoclonal IgG at 1:1000 dilution; anti-HSPA8 (HSC70), Abcam ab1427 rabbit polyclonal IgG at 1:1000 dilution; anti-HTT, Millipore MAB5492 mouse monoclonal IgG_1 at 1:1000 dilution and anti-GFP, Roche 11814460001 (clones 7.1 and 13.1) at 1:1000 dilution followed by detection with HRP-coupled anti-mouse and anti-rabbit antibodies and

chemoluminescence detection. Each knock-down and western blot experiment was verified in two biological repeats.

Supplemental References

Ahn, Y. Y., J. P. Bagrow, et al. (2010). Link communities reveal multiscale complexity in networks. Nature 466(7307): 761-764.

Bauer, D. F. (1972). Constructing confidence sets using rank statistics. Journal of the American Statistical Association 67: 687-690.

Berchtold, N. C., D. H. Cribbs, et al. (2008). Gene expression changes in the course of normal brain aging are sexually dimorphic. Proceedings of the National Academy of Sciences of the United States of America 105(40): 15605-15610.

Braakman, I. and N. J. Bulleid (2011). Protein folding and modification in the mammalian endoplasmic reticulum. Annual review of biochemistry 80: 71-99.

Brookmeyer, R., S. Gray, et al. (1998). Projections of Alzheimer's disease in the United States and the public health impact of delaying disease onset. American journal of public health 88(9): 1337-1342.

Chang, H. C., Y. C. Tang, et al. (2007). SnapShot: molecular chaperones, Part I. Cell 128(1): 212.

Harris, T. (2012). WormBase release WS232.

Harris, T. W., I. Antoshechkin, et al. (2010). WormBase: a comprehensive resource for nematode research. Nucleic acids research 38(Database issue): D463-467.

Heldens, L., R. P. Dirks, et al. (2010). Co-chaperones are limiting in a depleted chaperone network. Cellular and molecular life sciences : CMLS 67(23): 4035-4048.

Herndon, L. A., P. J. Schmeissner, et al. (2002). Stochastic and genetic factors influence tissue-specific decline in ageing C. elegans. Nature 419(6909): 808-814.

Hodges, A., A. D. Strand, et al. (2006). Regional and cellular gene expression changes in human Huntington's disease brain. Human molecular genetics 15(6): 965-977.

Kamath, R. S. and J. Ahringer (2003). Genome-wide RNAi screening in Caenorhabditis elegans. Methods 30(4): 313-321.

Liang, W. S., E. M. Reiman, et al. (2008). Alzheimer's disease is associated with reduced expression of energy metabolism genes in posterior cingulate neurons. Proceedings of the National Academy of Sciences of the United States of America 105(11): 4441-4446.

Link, C. D. (1995). Expression of human beta-amyloid peptide in transgenic Caenorhabditis elegans. Proceedings of the National Academy of Sciences of the United States of America 92(20): 9368-9372.

Loerch, P. M., T. Lu, et al. (2008). Evolution of the aging brain transcriptome and synaptic regulation. PloS one 3(10): e3329.

Moran, L. B., D. C. Duke, et al. (2006). Whole genome expression profiling of the medial and lateral substantia nigra in Parkinson's disease. Neurogenetics 7(1): 1-11.

Sayers, E. W., T. Barrett, et al. (2012). Database resources of the National Center for Biotechnology Information. Nucleic acids research 40(Database issue): D13-25.

Silva, M. C., S. Fox, et al. (2011). A genetic screening strategy identifies novel regulators of the proteostasis network. PLoS genetics 7(12): e1002438.

Tang, Y. C., H. C. Chang, et al. (2007). SnapShot: molecular chaperones, Part II. Cell 128(2): 412.